# Direct capture, inhibition and crystal structure of HsaD (Rv3569c) from M. tuberculosis

Sarah Barelier, Romain Avellan, Giri Raj Gnawali, Patrick Fourquet, Véronique Roig-Zamboni, Isabelle Poncin, Vanessa Point, Yves Bourne, Stéphane Audebert, Luc Camoin, et al.

# Direct capture, inhibition and crystal structure of HsaD (Rv3569c) from *M. tuberculosis*

Sarah Barelier[a], Romain Avellan[b], Giri Raj Gnawali[c], Patrick Fourquet[d], Véronique Roig-Zamboni[a], Isabelle Poncin[b], Vanessa Point[b], Yves Bourne[a], Stéphane Audebert[d], Luc Camoin[d], Christopher D. Spilling[c], Stéphane Canaan[b], Jean-François Cavalier[b,*], Gerlind Sulzenbacher[a,*]

[a] Aix-Marseille Univ., CNRS, AFMB, Marseille, France

[b] Aix-Marseille Univ., CNRS, LISM, IMM FR3479, Marseille, France

[c] Department of Chemistry and Biochemistry, University of Missouri-St. Louis, One University Boulevard, St. Louis, Missouri, 63121, United States

[d] Aix-Marseille Univ., INSERM, CNRS, Institut Paoli-Calmettes, CRCM, Marseille Protéomique, Marseille, France

* To whom correspondence should be addressed

E-mail address: jfcavalier@imm.cnrs.fr (J.-F. Cavalier); https://orcid.org/0000-0003-0864-8314

E-mail address: gerlind.sulzenbacher@univ-amu.fr (G. Sulzenbacher); https://orcid.org/0000-0003-4844-2820

**Running title**

Inhibition and structural characterization of HsaD

**Abbreviations**

ABPP, activity-based protein profiling; au, arbitrary unit; CC-ABPP, click chemistry ABPP; CyC, Cyclipostins and Cyclophostin analogues; HOPDA, 2-hydroxy-6-oxo-6-phenylhexa-2,4-dienoic acid; ILI, intrabacterial lipid inclusion; INH, isoniazid; $MIC_{90}$, minimal inhibitory concentration leading to 90% bacterial growth inhibition; REMA, resazurin microtiter assay; RMSD, root-mean-square deviation; TAG, triacylglycerols; TB, tuberculosis; $x_I$, inhibitor molar excess related to 1 mol of enzyme; $x_{I50}$, inhibitor molar excess leading to 50% enzyme inhibition.

**Keywords**

Activity-based protein profiling; Antituberculous molecules; Inhibition mechanism; Cholesterol metabolism; Cyclipostins & Cyclophostin

**Conflicts of Interest**

The authors declare no conflict of interest.

**ABSTRACT**

A hallmark of *Mycobacterium tuberculosis* (*M. tb*), the etiologic agent of tuberculosis, is its ability to metabolize host-derived lipids. However, the enzymes and mechanisms underlying such metabolism are still largely unknown. We previously reported that the Cyclophostin & Cyclipostins (**CyC**) analogs, a new family of potent antimycobacterial molecules, react specifically and covalently with (Ser/Cys)-based enzymes mostly involved in bacterial lipid metabolism. Here, we report the synthesis of new **CyC** alkyne-containing inhibitors (**CyC**$_{\mathbf{yne}}$) and their use for the direct fishing of target proteins in *M. tb* culture *via* bio-orthogonal click-chemistry activity-based protein profiling (CC-ABPP). This approach led to the capture and identification of a variety of enzymes, many of them involved in lipid or steroid metabolisms. One of the captured enzymes, HsaD (Rv3569c), is required for the survival of *M. tb* within macrophages and is thus a potential therapeutic target. This prompted us to further explore and validate, through a combination of biochemical and structural approaches, the specificity of HsaD inhibition by the **CyC** analogs. We confirmed that the **CyC** bind covalently to the catalytic Ser$^{114}$ residue, leading to a total loss of enzyme activity. These data were supported by the X-ray structures of four HsaD-**CyC** complexes, obtained at resolutions between 1.6-2.6 Å. The identification of mycobacterial enzymes directly captured by the **CyC**$_{\mathbf{yne}}$ probes through CC-ABPP paves the way to better understand and potentially target key players at crucial stages of the bacilli life-cycle.

## INTRODUCTION

Tuberculosis (TB), caused by *Mycobacterium tuberculosis* (*M. tb*), is still one of to the top-ten causes of death worldwide triggered by a bacterial pathogen. In 2020, nearly 1.5 million people died from TB and an additional 9.9 million contracted the disease [1].

A key feature of *M. tb* pathogenesis, as well as other pathogenic mycobacteria, is its ability to survive within macrophages. Numerous studies have highlighted the critical role of host-derived carbon sources, such as fatty acids and/or cholesterol, for *M. tb* to persist and replicate inside macrophages [2-5]. Accordingly, during infection, *M. tb* is able to hydrolyze host lipids, and to store them as triacylglycerols (TAG) in its own cytoplasm as intrabacterial lipid inclusions (ILIs). These ILI will then serve as a source of carbon and energy to sustain bacterial survival [2]. In addition to TAG, cholesterol catabolism also plays a central role in the infection process of *M. tb* [6, 7], as cholesterol is used as a carbon source during the survival of the bacillus inside macrophages [5, 8].

Collectively, the acquisition of lipids and cholesterol is essential for the long-term survival and persistence of *M. tb* [9, 10]. Consequently, the mycobacterial enzymes involved in such metabolisms are considered potential targets for TB drug discovery.

Most of these enzymes belong to the α/β-hydrolase fold superfamily [11], which includes hydrolases, oxidoreductases, transferases, lyases, ligases and isomerases. The hydrolase class covers a wide variety of enzymes, such as esterases, lipases, thioesterases, dienelactone hydrolases, epoxide hydrolases, peptidases, a 2-hydroxy-6-oxo-6-phenylhexa-2,4 dienoate hydrolase and haloalkane dehalogenases [11]. A conserved structural feature of these enzymes is the presence of a catalytic serine or cysteine residue in their active site.

Such (Ser/Cys)-based mycobacterial enzymes represent a promising class of potential therapeutic targets in the fight against TB [12]. Therefore, finding ways to identify, inhibit or control their activity may open the way to new chemotherapeutic developments against mycobacterial infections.

In this context, the discovery of covalent inhibitors has led to the development of a powerful chemoproteomic approach, termed activity-based protein profiling (ABPP), allowing the identification of bacterial (Ser/Cys)-based enzymes in complex proteomes [13].

We previously reported the development of Cyclophostin & Cyclipostins (**CyC**) analogs, a new family of potent antimycobacterial molecules reacting specifically and covalently with (Ser/Cys)-based enzymes [14, 15]. Among a set of 38 **CyC** analogs tested against *M. tb*, the Cyclophostin analogs **CyC$_{7\beta}$** and **CyC$_{8\beta}$** as well as the Cyclipostins analog **CyC$_{17}$** displayed potent anti-tubercular activity. Whereas **CyC$_{7\beta}$** exhibited promising activity against both extracellular and intracellular mycobacteria ($MIC_{90}$ of 37.2 and 5.0 µM, respectively), **CyC$_{8\beta}$** was mostly found to be active against intracellular bacteria ($MIC_{90}$ ~ 13.9 µM). Conversely, **CyC$_{17}$** was a potent inhibitor of extracellular growth ($MIC_{90}$ ~ 2.6 µM) with no activity against intracellular bacilli [15, 16]. A competitive ABPP approach using **CyC$_{17}$**-pretreated *M. tb* lysate and the ActivX™ Desthiobiotin-FP probe led to the identification of 23 distinct proteins as potential targets of this inhibitor, which were all (Ser/Cys)-based enzymes, most of them participating in *M. tb* lipid or cholesterol metabolism as well as cell wall biosynthesis [15, 16]. In particular, HsaD (2-hydroxy-6-oxo-6-phenylhexa-2,4-dienoate hydrolase, Rv3569c) was identified as a potential target of **CyC$_{17}$**. This protein catalyzes the hydrolytic cleavage of carbon-carbon bonds of the *meta*-cleavage product 4,5-9,10-diseco-3-hydroxy-5,9,17-trioxoandrosta-1(10),2-diene-4-oic acid (4,9-DHSA) in the cholesterol metabolic pathway [8] and is one of the four key enzymes involved in the degradation of the A/B rings of cholesterol (*i.e.*, HsaA, Rv3567; HsaB, Rv3570; HsaC, Rv3568; and HsaD) [8]. Moreover, studies using transposon mutagenesis have shown that HsaD was required for the survival of *M. tb* within macrophages [3, 9].

However, this latter competitive ABPP approach for target identification in cell lysates [16] presented the major disadvantage of being indirect and not applied on living cells, with the risk of identifying proteins present in the lysate but not targeted *in vivo*.

Here, we report the synthesis of two new analogs of **CyC$_{17}$** containing a terminal alkyne function (*i.e.*, **CyC$_{yne}$**) and describe their use for the direct capture of target proteins in a living *M. tb* culture using a direct click chemistry ABPP approach (CC-ABPP) [17-20]. Since HsaD appeared also as a target of these new **CyC$_{yne}$** probes, and given its potential as therapeutic target [21], we further explore and validate, through a combination of biochemical and structural approaches, the specificities of HsaD inhibition by the **CyC** analogs.

## RESULTS

### Synthesis, antibacterial activity and target enzyme identification *via* activity-based protein profiling using CyC$_{yne}$ probes

The monocyclic enol-phosphate **CyC$_{31yne}$** and phosphonate **CyC$_{32yne}$** probes were prepared using the transesterification protocol, as previously published [22]. The ester exchange reaction process with the monocyclic phosphate **CyC$_{16}$** [15, 23] or phosphonate **CyC$_{4}$** [15, 22] methyl ester was achieved in presence of excess of 11-bromoundec-1-yne **1** [24] and TBAI in refluxing toluene or 1,4-dioxane to give the corresponding alkynyl phosphate **CyC$_{31yne}$** or phosphonate **CyC$_{32yne}$** derivative in 43-44% yields (**Fig. 1A**). The corresponding alkyl parent molecules, **CyC$_{31}$** and **CyC$_{32}$**, were obtained from similar reaction with 1-bromoundecane in 38-42% yields.

The antimicrobial potency of the two **CyC$_{yne}$** as compared to **CyC$_{31}$** and **CyC$_{32}$** was evaluated against *M. tb* mc$^2$6230. The minimal inhibitory concentration leading to 90% bacterial growth inhibition (*i.e.*, MIC$_{90}$) was determined by the resazurin microtiter assay (REMA) [16, 25, 26]. Similar antibacterial activities against *M. tb* mc$^2$6230 were obtained for each pair, *i.e.*, **CyC$_{31}$** / **CyC$_{31yne}$** (5.3 / 7.7 µM) and **CyC$_{32}$** / **CyC$_{32yne}$** (5.4 / 7.2 µM), respectively (**Fig. 1A**). Interestingly, **CyC$_{31}$** and **CyC$_{32}$** exhibited MIC$_{90}$ values of the same order of magnitude than that of **CyC$_{17}$** (2.6 µM) against *M. tb* [16, 26].

Based on these results, **CyC$_{31yne}$** and **CyC$_{32yne}$** were used as probes in a click-chemistry activity-based protein profiling (CC-ABPP) strategy (**Fig. 1B**) [27]. Each **CyC$_{yne}$** probe was first incubated with

*M. tb* culture followed by cell lysis. Then, subsequent bio-orthogonal click-chemistry reaction led to the formation of a stable triazole cycle between the **CyC$_{yne}$**-enzyme complex and the Desthiobiotin-$N_3$ *via* the copper(I)-catalyzed Huisgen's 1,3-dipolar cycloaddition reaction [28]. After enrichment on streptavidin agarose-beads, the mixtures were further digested with trypsin. The resulting peptides were analyzed by liquid chromatography-tandem mass spectrometry (LC-MS/MS) followed by label free quantification analysis. The comparative proteomic analysis between a control sample (*i.e.*, DMSO-treated *M. tb* cells for non-specific binding to streptavidin agarose-beads) and **CyC$_{yne}$**-treated samples led to the identification of 155 and 159 target enzymes with **CyC$_{31yne}$** and **CyC$_{32yne}$**, respectively, when applying *p*-value $\leq$ 0.01 and fold-change $\geq$ 1.2 thresholds on the proteomics analysis results (**Fig. 1C** and **Tables S1-S2**).

As expected from their closely related chemical structure and the well-known mechanism of action of such enolphosphorus derivatives [14, 15], a comparable proteomic profile was obtained with the two **CyC$_{yne}$** probes (**Fig. 1C** and **Tables S1-S2**), as depicted in the Venn diagram and the protein functional categorization (**Fig. 1C-b,c** and **Table S3**). Interestingly, while both inhibitors share 139 common targets, 19 and 23 additional specific target enzymes were obtained with **CyC$_{31yne}$** and **CyC$_{32yne}$**, respectively (**Fig. 1C-b** and **Table S3**), thereby demonstrating some degree of selectivity between the two **CyC** inhibitors. Noteworthily, as depicted in the Volcano Plot (**Fig. 1C-a**), 20 out of the 23 (Ser/Cys)-based enzymes previously identified with **CyC$_{17}$** in a competitive ABPP approach [16] were also captured by the **CyC$_{31yne}$** probe. Notably, if nine enzymes (AdhB, BpoC, CaeA, GlyA1, LipM, LipN, Rv1367c, SerA1 and UmaA) were found below the 1.2-fold-change threshold, eleven proteins (Ag85A/C, AmiB2, HsaD, LipH, LipV, Rv0045c, Rv0183, Rv1730c, Rv1984c and TesA) were detected above this threshold (**Fig. 1C-a**). Eighteen of these latter 20 enzymes were also captured by **CyC$_{32yne}$** with a similar distribution using the same 1.2-fold-change threshold. Of interest, the carbon-carbon hydrolase HsaD involved in cholesterol metabolism was only captured by the alkylphosphate inhibitor **CyC$_{31yne}$** and not by its alkylphosphonate counterpart **CyC$_{32yne}$** (**Table S3**).

The fact that HsaD was found to be essential for intramacrophage survival of *M. tb* [3] and that its overexpression was associated with increased resistance levels to **CyC$_{17}$** [16], prompted us to further investigate its biochemical and structural interactions with **CyC$_{17}$**, the new **CyC$_{31}$** and **CyC$_{32}$**, as well as with two inhibitors of intracellular *M. tb* growth **CyC$_{7\beta}$** and **CyC$_{8\beta}$** [16].

**Covalent inhibition of the HsaD MCP hydrolase activity.**

HsaD was previously characterized as a member of the *meta*-cleavage product (MCP) hydrolase class of enzymes that catalyzes the hydrolytic cleavage of a carbon-carbon bond through a serine protease-like catalytic triad [29, 30]. HsaD was reported to exhibit a high specificity for the steroid 4,9-DHSA within the cholesterol metabolic pathway [8].

To test the hypothesis that the **CyC** analogs inhibit HsaD activity, we first cloned *hsaD* (*rv3569c*) into a pVV16 vector, and the recombinant protein was produced in *M. smegmatis*. HsaD was purified to homogeneity by successive nickel affinity and size-exclusion chromatography steps, leading to 5-10 mg of pure recombinant protein per liter of culture. The protein was further concentrated up to 7.5 mg/mL, the highest concentration used for crystallographic experiments. Its purity as well as the expected molecular weight (~33 kDa) were confirmed by 15% SDS-PAGE (**Fig. 2A**) and global mass spectrometry (**Fig. 2D**).

To investigate the inhibitory potency of **CyC$_{17}$**, **CyC$_{31}$**, **CyC$_{32}$**, as well as **CyC$_{7\beta}$** and **CyC$_{8\beta}$** (**Fig. 2B**), the purified protein was incubated at room temperature with each inhibitor at various inhibitor molar excess ($x_I$). The residual enzyme activity was then measured using a MCP hydrolase activity assay with the synthetic substrate 2-hydroxy-6-oxo-6-phenylhexa-2,4-dienoic acid (HOPDA) [30]. The variation in HsaD residual activity allowed determination of the inhibitor molar excess leading to 50% enzyme inhibition, *i.e.*, $x_{I50}$ value [31, 32]. Thereby, a $x_{I50}$ value of 0.5 is synonymous with a 1:1 stoichiometric ratio between the inhibitor and the enzyme, and is therefore the highest level of inhibitory activity that can be achieved. In good agreement with the CC-ABPP results, **CyC$_{32}$** failed to inhibit HsaD activity even at high molar excess $x_I$ of 80 (*i.e.*, 14.4±0.10% inhibition). On the other

hand, a dose-dependent inhibition was observed with all the other four **CyC** compounds (**Fig. 2C**). In terms of molar excess of inhibitor, the **CyC$_{7\beta}$**, **CyC$_{8\beta}$** and **CyC$_{31}$** were 2.7-3.4 times more active towards HsaD than **CyC$_{17}$**, as judged by their respective $x_{I50}$ values of 1.19, 1.52, 1.44 and 4.09, respectively.

Next, we confirmed the covalent nature of the inhibition using MALDI-TOF mass spectrometry. In the presence of **CyC$_{7\beta}$** (374.2 Da), a mass increment of +370.8 was observed as compared to the global mass of untreated HsaD (**Fig. 2D**). Mass spectra of tryptic digestion in the 1300-1900 Da interval further confirmed the covalent binding by highlighting the $V^{108}$PLVGNS$^{114}$LGGGTAVR$^{122}$ peptide, which contains the catalytic $Ser^{114}$ in its native ($[M+H]^+$ = 1396.888 Da) and modified ($[M+H]^+$ = 1771.089 Da) forms (**Fig. 2E**). Additionally, MS/MS spectrum of the modified peptide confirmed the specific coupling of **CyC$_{7\beta}$** to the $Ser^{114}$ residue with a gap of ~69 Da corresponding to $Ser^{114}$ without the hydroxyl group as well as a neutral loss of around +374.4 Da. These data clearly support the formation of a covalent HsaD-**CyC$_{7\beta}$** complex at the catalytic $Ser^{114}$ (**Fig. 2F**). Similar results were obtained with **CyC$_{8\beta}$** following tryptic digestion, with a mass difference between the native and modified peptides of +402.23 Da (**Fig. 3A**). These results are consistent with the known and irreversible mechanism of action of such phosphonate compounds, as previously demonstrated using pure mycobacterial lipolytic enzymes [32-34].

With respect to the phosphate analog **CyC$_{31}$**, the observed +237.8 Da mass shift increment was 138.4 Da lower than its theoretical molecular mass of 376.2 Da (**Fig. 2D**). Peptide mass fingerprinting of the HsaD-**CyC$_{31}$** adduct followed by the MS/MS analysis of the $V^{108}$-$R^{122}$ modified peptide (**Fig. 2E**) confirmed the covalent binding to $Ser^{114}$ as well as the mass difference of around +234.2 Da. Such a difference in mass, also observed with **CyC$_{17}$** (304.2 Da *vs*. 446.28 Da – **Fig. 3B**) is in agreement with previous studies of the thioesterase TesA and the Antigen 85 complex [33, 34]. Here, after phosphorylation of the HsaD-$Ser^{114}$ catalytic serine by **CyC$_{31}$** or **CyC$_{17}$**, further rearrangement of the covalently bound inhibitor occurs, resulting in the loss of the methyl 2-acetyl-4-hydroxybutanoate moiety to reach a stable thermodynamic state (**Fig. 2F** and **Fig. 3B**). In addition, this mechanism is

not only perfectly in line with the data generated by the proteomic experiments, but above all it was further corroborated by the crystal structure of the **CyC$_{31}$**-HsaD complex as outlined below.

### Crystal structures of HsaD

The structure of native HsaD was solved at a high resolution (1.96 Å), and is identical to the one described by Lack et al. (PDB: 2VF2) [21, 35], with a root-mean-square deviation (RMSD) of 0.317 over 259 alpha carbon atoms; making our HsaD structure the best resolution obtained so far. Crystals of native HsaD belong to space group $P222_1$ with average unit cell axes of 76.8 × 87.4 × 106.2 Å and two molecules per asymmetric unit. The biological assembly is a homo-tetramer, which can be generated by application of a crystallographic two-fold axis. The two monomers present in the asymmetric unit are nearly identical (RMSD 0.248 Å over 266 alpha carbon atoms) and display an α/β-hydrolase fold, which contains the active site made-up by the catalytic triad Ser$^{114}$, Asp$^{241}$ and His$^{269}$ [30]. Residues 7-290 were built in both chains, while the first six residues as well as the 6×His-tag at the C-terminus were not modeled due to lack of experimental evidence.

Structural studies of HsaD in the presence of **CyC$_{7\beta}$**, **CyC$_{8\beta}$**, **CyC$_{17}$** and **CyC$_{31}$** led to well-defined structures of enzyme-inhibitor complexes with very high resolutions in the 1.62 Å to 2.20 Å range. Crystals of HsaD in complex with **CyC$_{8\beta}$**, **CyC$_{17}$** and **CyC$_{31}$** belong to the same space group as native HsaD with similar unit cell axes and two molecules per asymmetric unit. In contrast, crystals of HsaD in complex with **CyC$_{7\beta}$** belong to space group $P2_12_12$ with unit cell axes of 76.9 × 78.4 × 92 Å. Data collection and refinement statistics for all structures are shown in **Table 1**.

The crystal structures of each complex were compared to that of native HsaD. No major conformational changes induced by inhibitor-binding could be observed (overall RMSD with respect to native HsaD of 0.09 to 0.12 Å for **CyC$_{8\beta}$**, **CyC$_{17}$** and **CyC$_{31}$**, and 0.47 Å for **CyC$_{7\beta}$**, which belongs to a different space group) (**Fig. 4A**). The three catalytic residues Ser$^{114}$, Asp$^{241}$ and His$^{269}$ adopt the same conformations in all complexes (**Fig. 4B**). The main differences are observed at the level of the side-chains of Asn$^{54}$, Asn$^{113}$, Leu$^{158}$ and Met$^{177}$ that are within close proximity of the catalytic serine

Ser$^{114}$. Additionally, the large movement of Met$^{177}$ in the HsaD-**CyC$_{7\beta}$** complex induces a cascade of conformational changes which pushes away the oppositely lying side-chains of Ser$^{56}$ and Arg$^{57}$ and leads to the fusion of two short helices into a single, bent helix (**Fig. 4C**). However, these differences, which are not caused by crystal packing artefacts, do not affect the overall structure of the active site of HsaD.

Covalent binding of all **CyC** compounds to Ser$^{114}$ was confirmed by careful examination of the electron density around Ser$^{114}$. In all four complexes, electron density for the phosphate group covalently linked to Ser$^{114}$ was clearly visible in both chain A and chain B.

Clear electron density can be seen for nearly the entire structure of the Cyclophostin analog **CyC$_{7\beta}$** in both monomers, although the end of the alkyl chain cannot be modeled with certainty (**Fig. 5A**). The observed electron density agrees with ring aperture, confirming that the compound has reacted with Ser$^{114}$ (**Fig. 2F**). The observed distance of about 1.5 Å between the phosphorus atom of **CyC$_{7\beta}$** and the side-chain oxygen of Ser$^{114}$ clearly attests that in the crystal, the ligand is covalently bound. The phosphonate group of **CyC$_{7\beta}$** forms hydrogen-bonds with the backbone atoms of Gly$^{45}$ and Leu$^{115}$, and with the side-chain of His$^{269}$, which in turn is stabilized *via* hydrogen-bonding to Asp$^{241}$ (**Fig. 5B-D**). The rest of the molecule forms few interactions with the enzyme, except for a hydrogen bond between a carbonyl of **CyC$_{7\beta}$** and the backbone of Gly$^{141}$. The long aliphatic chain of **CyC$_{7\beta}$** is stabilized by hydrophobic interactions involving in particular the side chains of Leu$^{158}$, Met$^{208}$ and Phe$^{212}$.

For **CyC$_{8\beta}$**, which differs from **CyC$_{7\beta}$** only by two extra carbon atoms, only the covalent phosphonate head with its methoxy group was modeled, as the observed electron density was incomplete. The position of the phosphonate confirms the covalent nature of the [Ser$^{114}$-O$\gamma$/P] bond (1.6 Å) and is compatible with a binding comparable to that of **CyC$_{7\beta}$**. Interactions similar to the HsaD-**CyC$_{7\beta}$** complex are observed between the phosphonate head of the compound and the active site residues. Finally, crystals of the HsaD-**CyC$_{8\beta}$** complex that were re-solubilized and subjected to mass spectrometry analysis, show a shift corresponding to **CyC$_{8\beta}$** molecular weight (+402.23 Da – **Fig.**

**3A**), indicating that the compound is present in full-length within the crystal, even though it was not observed entirely in the electron density, possibly due to radiation damage or conformational flexibility.

Regarding the Cyclipostins analog **CyC$_{17}$**, again the electron density does not allow confident placement of the entire compound in the electron density and only the phosphate head covalently bound to Ser$^{114}$ was modeled ([Ser$^{114}$-Oγ/P] distance ~1.5 Å). Finally, in the HsaD-**CyC$_{31}$** complex, the crystal structure confirmed the mass spectrometry data (**Fig. 2D-F**). Indeed, the inhibitor, whose aliphatic chain contains 5 carbon atoms less compared to **CyC$_{17}$**, has lost its β-ketoester moiety. The hydrolyzed molecule is clearly visible in the electron density (**Fig. 5A**) and covalent binding is confirmed ([Ser$^{114}$-Oγ/P] distance ~1.5 Å). Here, the phosphate head hydrogen-bonds with the backbones of Gly$^{45}$ and Leu$^{115}$, with the side-chain of His$^{269}$, itself stabilized by Asp$^{241}$ and with two water molecules. The long aliphatic chain is stabilized by hydrophobic interaction with the side-chains of Leu$^{158}$, Met$^{208}$ and Phe$^{212}$ (**Fig. 5B-D**).

Overall, the binding modes are highly similar between the Cyclophostin analog **CyC$_{7β}$** and the Cyclipostins analog **CyC$_{31}$**, involving the same active site residues.

### *In silico* molecular docking study

In order to better understand the absence of inhibitory activity of **CyC$_{32}$** at the molecular level, complementary *in silico* molecular docking experiments were conducted as described previously [16, 32] using our HsaD-**CyC$_{31}$** crystal structure (PDB ID: 7ZM4) as receptor (**Fig. 6**). Docking runs were performed using the Autodock Vina program [36] after removing the bound **CyC$_{31}$** and replacing the catalytic Ser$^{114}$ by a glycine residue in order to enable the docked inhibitor to adopt a suitable position corresponding to the prebound intermediate before the nucleophilic attack in the active site [16, 32]. For **CyC$_{32}$**, the best scoring position obtained (*i.e.* lowest energy complex) places this compound at the entrance of the active site cleft, with a predicted binding energy value $\Delta E_{\mathbf{CyC32}} = -7.3$ kcal/mol (**Fig. 6A**). In this nonproductive orientation, the phosphorus atom of the docked **CyC$_{32}$** would indeed

be found in an opposite and unfavorable position at a 9.5 Å distance from the catalytic $Ser^{114}$, thus excluding the occurrence of any covalent interaction (**Fig. 6B**). In contrast, the same *in silico* docking experiment performed with **CyC31** resulted in a best scoring position showing the reactive phosphorus atom at a 1.6 Å distance from the catalytic $Ser^{114}$, therefore facilitating the formation of a covalent bond, with a predicted binding energy value $\Delta E_{\mathbf{CyC31}_{docked}} = -7.8$ kcal/mol (**Fig. 6B**). Comparison of this generated **CyC31***docked* top ranked docking pose with the binding geometry observed in the HsaD-**CyC31** crystal structure revealed of 0.7 Å deviation between the two reactive phosphorus atoms (**Fig. 6C**). This redocking/crossdocking experiment thus confirms the validity and reliability of our computational approach. In addition, using a similar *in silico* approach with the reported crystal structure of HsaD bound to 3,5-dichloro-4-hydroxybenzoic acid (PDB: 5JZS - 2.27 Å resolution [21]), we had previously demonstrated that **CyC17** adopted a productive orientation close to the catalytic $Ser^{114}$ ($\Delta E_{\mathbf{CyC17}} = -7.4$ kcal/mol; [$Ser^{114}$-Oγ/P] distance ~2.3 Å) [16]. A good level of concordance was also observed between the favorable docked conformation of **CyC17** and the 3D structure of the covalently bound **CyC31**-$Ser^{114}$ in HsaD active site (**Fig. 6D**).

Overall, such *in silico* molecular docking results not only corroborate our experimental biochemical data, but above all provide some clues that may explain the absence of inhibitory activity of **CyC32** towards HsaD.

## DISCUSSION

Compounds that specifically target mycobacterial (Ser/Cys)-based enzymes represent novel and promising antibacterial agents, offering supplementary therapeutic options [15, 20, 37]. In this regard, we have shown that Cyclophostin & Cyclipostins analogs (**CyC**) are potent anti-mycobacterial multi-target compounds leading to the arrest of *M. tb* growth either in broth medium or inside infected macrophages, by impairing simultaneously the activity of various (Ser/Cys)-based enzymes participating in important physiological processes related to lipid metabolism [15]. More specifically, the physiological processes related to host-lipid metabolism (cholesterol and fatty acids) are critical

to the *M. tb* infectious life-cycle for propagation of the infection, establishment of the dormancy state and reactivation of the disease [2, 38]. Therefore, finding ways to identify and inhibit the enzymes involved in such metabolic processes in *M. tb* would open new opportunities to treat TB.

To address this vital issue, we synthesized novel **CyC** alkyne-containing inhibitors (*i.e.*, **CyC$_{yne}$**), analogous of the best **CyC$_{17}$** extracellular growth inhibitor [15]. We showed that these new activity-based probes represent very powerful and highly valuable tools to identify mycobacterial (Ser/Cys)-based enzyme by fishing them directly from a living *M. tb* culture. Our endeavor was comforted by the fact that both phosphate **CyC$_{31yne}$** and phosphonate **CyC$_{32yne}$** analogs share 136 common targets. Notably, most of the 23 (Ser/Cys)-based enzymes previously identified through competitive ABPP with **CyC$_{17}$** and the ActivX™ Desthiobiotin-FP probe [16] were also captured, confirming the robustness of this bio-orthogonal click chemistry ABPP direct approach. Such a result was however expected due to the very close chemical structure with similar hydrophobic properties (*i.e.*, mean Log P = 4.72 ± 0.28 – **Fig. 2B**), and identical mechanism of inhibition of **CyC$_{31yne}$** and **CyC$_{32yne}$**. Nevertheless, a set of 19 and 23 specific targets for **CyC$_{31yne}$** and **CyC$_{32yne}$**, respectively, were also obtained (**Fig. 1A**). The fact that some enzymes were captured with one **CyC$_{yne}$** and not the other will be due to the chemical properties of the phosphate *vs*. phosphonate chemical groups, thus emphasizing some selective inhibitory activity.

Among the **CyC** target enzymes, HsaD (Rv3569c) which is involved in the cholesterol metabolism pathway [8] and is also essential for *M. tb* survival inside macrophages [3, 9], was specifically captured, first by **CyC$_{17}$** [16], and here by **CyC$_{31yne}$**, but not by **CyC$_{32yne}$**. This guided our biochemical and structural research effort to investigate the interactions of HsaD with the Cyclipostins analogs **CyC$_{17}$**, **CyC$_{31}$** and **CyC$_{32}$**, as well as with the Cyclophostin analogs **CyC$_{7\beta}$** and **CyC$_{8\beta}$** that previously showed promising activity against intracellular mycobacteria [16].

Here, a combination of complementary and orthogonal approaches provides a clear overview of the interactions between HsaD and the five **CyC** compounds. We demonstrated that HsaD is not inhibited by **CyC$_{32}$** (**Fig. 2C**) and provided clues that this lack of inhibition may result from a non-productive

binding of the enolphosphorus core of **CyC$_{32}$** located at the entrance of the active site crevice, opposite Ser$^{114}$ (**Fig. 6A-B**). Such positioning would thus prevent any reaction with the catalytic serine, in agreement with the CC-ABPP experiment (**Fig. 1**). In contrast, biochemical and mass spectrometry experiments have confirmed the covalent binding of the two Cyclipostins analogs **CyC$_{17}$** and **CyC$_{31}$**, but also of the Cyclophostin analogs **CyC$_{7\beta}$** and **CyC$_{8\beta}$** to the catalytic Ser$^{114}$, leading to full inhibition of HsaD enzymatic activity (**Fig. 2**). The observation of *in vitro* inhibition of HsaD by **CyC$_{7\beta}$** and **CyC$_{8\beta}$** strengthens our previous findings pointing towards *M. tb* bacterial clearance from infected macrophages, as observed in *ex vivo* experiments in the presence of these two inhibitors [16]. Indeed, it is tempting to consider that intracellular *M. tb* growth inhibition may result at least in part from the inactivation of this enzyme, which is essential for intra-macrophagic bacterial survival [3].

Moreover, all data (dose response curves, global mass modification and peptide mass fingerprint on the digested HsaD-**CyC** adducts, as well as the corresponding crystal structures) converge to the same mechanism of covalent inhibition through phosphorylation of the catalytic Ser$^{114}$, thereby abolishing HsaD enzymatic activity. Remarkably, and as previously observed in the inhibited Ag85C-**CyC$_{17}$** and TesA-**CyC$_{17}$** complexes [33, 34], after phosphorylation of the serine by **CyC$_{17}$** or **CyC$_{31}$**, the two phosphates undergo a partial hydrolysis resulting in rearrangement of the inner structure of the bound inhibitors and the release of their methyl 2-acetyl 4-hydroxybutyrate group. Such chemical modification can undoubtedly be considered as the signature of the reactivity of these Cyclipostins phosphate analogs with (Ser/Cys)-based enzymes.

Finally, in the present study, a click-chemistry ABPP approach using newly synthesized **CyC$_{yne}$** probes has allowed the direct capture of enzymes playing a crucial role in lipid or steroid metabolism in *M. tb* life cycle. The structural results also underline the potency as well as the added value of using the **CyC$_{yne}$** probes to identify, *via* activity-based profiling approaches, novel targets to fight TB infection.

Overall, our results confirm that the **CyC** inhibitors are multi-target compounds leading to the inhibition of *M. tb* growth through the inhibition of various mycobacterial (Ser/Cys)-based enzymes involved in important physiological processes. Moreover, given their non-toxicity towards mammalian cells at concentrations up to 100 µM [16], the **CyC$_{yne}$** activity-based probes represent useful tools to better understand the metabolic pathways used by *M. tb* to catabolize host-derived lipids (cholesterol and fatty acids) for its survival. Notably, the identification of key enzymes inactivated by our probes and involved in the accumulation and consumption of intrabacterial lipid inclusions (ILI) at key stages of bacterial development [2] will provide highly valuable data and reveal new potential therapeutic targets for the elimination of actively replicating or latent bacilli from infected individuals.

## MATERIALS AND METHODS

### Compound synthesis

***General Experimental.*** All reactions were carried out in oven dried glassware under an atmosphere of argon unless otherwise noted. $^{1}H$ $^{13}C$ and $^{31}P$ NMR spectra were recorded at 300, 75 and 121 MHz, respectively. $^{1}H$ NMR spectra are referenced to $CDCl_3$ (7.27 ppm), $^{13}C$ NMR spectra are referenced to $CDCl_3$ (77.23 ppm), and $^{31}P$ NMR spectra are referenced to external $H_3PO_4$. Coupling constants, *J*, are reported in Hz. Analytical thin-layer chromatography (TLC) analyses were performed on silica gel plates $60PF_{254}$. Visualization was accomplished with UV light, $KMnO_4$ solution, or iodine. The **CyC$_{7\beta}$**, **CyC$_{8\beta}$**, and **CyC$_{17}$** were synthesized as described previously [23, 32]. Stock solutions (10 mM) of the **CyC** compounds were prepared in dimethyl sulfoxide (DMSO) and stored at 4°C.

***Methyl 4-methyl-2-(undec-10-yn-1-yloxy)-6,7-dihydro-1,3,2-dioxaphosphepine-5-carboxylate 2-oxide (CyC$_{31yne}$)***. To a solution of monocyclic phosphate ester **CyC$_{16}$** [15, 23] (0.100 g, 0.421 mmol) in 1,4-dioxane (1 mL) was added the solution of 11-bromoundec-1-yne (**1**) [24] (215 mg, 0.928 mmol) in 1,4-dioxane (1 mL). Solid $n$Bu$_4$NI (0.016 g, 0.042 mmol) was added and the solution was heated to reflux for 7 h when completion of reaction was observed by TLC and $^{31}P$ NMR spectroscopy. The solution was concentrated under reduced pressure and the crude mixture was purified using column chromatography ($SiO_2$, 50% EtOAc in hexane) to give the title compound (0.067 g, 43%) viscous green liquid. IR(neat) 2925, 2853, 1716, 1644, 1284 $cm^{-1}$; $^{1}H$ NMR (300 MHz, $CDCl_3$) δ 4.44-4.30 (m, 1H), 4.26-4.09 (m, 3H), 3.78 (s, 3H), 3.10-2.76 (m, 2H), 2.37 (s, 3H), 2.19 (td, $J_{HH}$ = 7.0, 2.6 Hz, 2H), 1.95 (t, $J_{HH}$ = 2.6 Hz, 1H), 1.76-1.66 (m, 2H), 1.55-1.47 (m, 2H), 1.43-1.22 (m, 10H); $^{13}C$ NMR (75 MHz, $CDCl_3$) δ 167.2 (d, $J_{HP}$ = 1.8 Hz), 161.1 (d, $J_{CP}$ = 9.6 Hz), 115.5 (d, $J_{CP}$ = 3.8 Hz), 84.8, 69.2 (d, $J_{CP}$ = 6.1 Hz), 68.3, 68.2, 52.2, 30.3 (d, $J_{CP}$ = 6.6 Hz), 29.4, 29.1, 29.1, 28.8, 28.5, 28.2, 25.4, 20.4 (d, $J_{CP}$ = 3.8 Hz), 18.5; $^{31}P$ NMR (121 MHz, $CDCl_3$); δ -10.77; HRMS (ESI, $MH^+$) calcd for $C_{18}H_{30}O_6P$ 373.1780, found 373.1775 and ($MNa^+$) calcd for $C_{18}H_{29}O_6PNa$ 395.1599 found 395.1594.

***Methyl 4-methyl-2-(undecyloxy)-6,7-dihydro-1,3,2-dioxaphosphepine-5-carboxylate 2-oxide (CyC$_{31}$)***. To a solution of monocyclic phosphate ester **CyC$_{16}$** (0.100 g, 0.421 mmol) in 1,4-dioxane (1 mL) was added a solution of bromoundecane (0.366 mL, 1.63 mmol) followed by the addition of *n*Bu$_4$NI (0.020 g, 0.054 mmol) in 1,4-dioxane (1 mL). The resulting solution was heated to reflux for 4 h when the completion of reaction was observed by TLC and $^{31}$P NMR spectroscopy. The solution was concentrated *in vacuo* and the residue was purified using column chromatography ($SiO_2$, 50% EtOAc in hexane) to give **CyC$_{31}$** viscous liquid (0.059 mg, 38%). IR (neat) 2921, 2851, 1717, 1644, 1287 cm$^{-1}$; $^1$H NMR (300 MHz, $CDCl_3$) δ 4.434-4.28 (m, 1H), 4.23-4.08 (m, 3H), 3.75 (s, 3H), 3.06-2.76 (m, 2H), 1.76-1.64 (m, 2H), 1.40-1.17 (m, 16H), 0.86 (d, $J_{HH}$ = 6.4 Hz, 3H); $^{13}$C NMR (75 MHz, $CDCl_3$) δ 167.2 (d, $J_{HP}$ = 1.9 Hz), 161.1 (d, $J_{HP}$ = 9.6 Hz), 115.4 (d, $J_{HP}$ = 3.8 Hz), 84.8, 69.2 (d, $J_{HP}$ = 6.0 Hz), 68.2, 68.2, 52.2, 31.9, 30.3 (d, $J_{CP}$ = 6.6 Hz), 29.6, 29.5, 29.4, 29.1, 28.2, 22.7, 20.4 (d, $J_{CP}$ = 3.8 Hz), 14.2; $^{31}$P NMR (121 MHz, $CDCl_3$); δ -10.8; HRMS (ESI, $MH^+$) calcd for $C_{18}H_{34}O_6P$ 377.2093, found 377.2088.

***Methyl 7-methyl-2-(undec-10-yn-1-yloxy)-3,4,5-trihydro-1,2-oxaphosphepine-6-carboxylate 2-oxide (CyC$_{32yne}$)***. To a solution of monocyclic phosphonate ester **CyC$_4$** [15, 22] (0.085 g, 0.363 mmol) in dry toluene (1 mL) was added a solution of solution 11-bromoundec-1-yne (**1**) [24] (0.185 g, 0.798 mmol) in dry toluene (1 mL). Solid *n*Bu$_4$NI (0.013 g, 0.036 mmol) was added and heated the mixture was heated to reflux for 4 h when completion of reaction was observed by TLC and $^{31}$P NMR spectroscopy. The solution was concentrated under reduced pressure and the crude mixture was purified using column chromatography ($SiO_2$, 50% EtOAc in hexanes) to give the title compound (0.059 g, 44%) as viscous liquid. IR (neat) 2926, 2854, 1713, 1643 cm$^{-1}$; $^1$H NMR (300 MHz, $CDCl_3$) δ 4.19-4.05 (m, 2H), 3.73 (s, 3H), 2.68-2.42 (m, 2H), 2.31 (s, 3H), 2.18-2.08 (m, 3H), 2.06-2.00 (m, 1H), 1.96-1.85 (m, 3H), 1.74-1.60 (m, 2H), 1.58-1.42 (m, 2H), 1.34-1.28 (br, 10H); $^{13}$C NMR (75 MHz, $CDCl_3$) δ 168.2, 159.4 (d, $J_{CP}$ = 7.8 Hz), 119.2 (d, $J_{CP}$ = 4.6 Hz), 84.8, 68.3, 66.2 (d, $J_{CP}$ = 7.1 Hz), 52.0, 30.5 (d, $J_{CP}$ = 6.1 Hz), 29.5, 29.2, 29.1, 28.8, 28.6, 27.7, 26.4 (d, $J_{CP}$ = 2.5 Hz), 25.9, 25.6, 21. (d, $J_{CP}$ = 7.5 Hz), 21.1 (d, $J_{CP}$ = 1.6 Hz), 18.5; $^{31}$P NMR (121 MHz, $CDCl_3$) δ 23.2; HRMS (ESI,

$MH^+$) calcd for $C_{19}H_{32}O_5P$ 371.1987 found 371.1984 and ($MNa^+$) calcd for $C_{19}H_{31}O_5PNa$ 393.1807 found 393.1801.

***Methyl 7-methyl-2-(undecyloxy)-3,4,5-trihydro-1,2-oxaphosphepine-6-carboxylate 2-oxide (CyC$_{32}$)***. To a solution of monocyclic phosphonate ester **CyC$_4$** (0.145 g, 0.619 mmol) in toluene (1 mL) was added a solution of bromoundecane (0.0.415 mL, 1.85 mmol) followed by the addition of *n*$Bu_4NI$ (0.023 g, 0.062 mmol) in toluene (1 mL). The resulting solution was heated to reflux for 4 h when the completion of reaction was observed by TLC and $^{31}P$ NMR spectroscopy. The solution was concentrated *in vacuo* and the residue was purified using column chromatography ($SiO_2$, 50% EtOAc in hexane) to give **CyC$_{32}$** viscous liquid (0.097 g, 42%). IR (neat) 2921, 2852, 1714, 1644 $cm^{-1}$; $^1H$ NMR (300 MHz, $CDCl_3$) δ 4.20-4.03 (m, 3H), 3.72 (s, 3H), 2.69-2.48 (m, 2H), 2.38 (s, 3H), 2.30-1.82 (m, 5H), 1.71 – 1.59 (m, 3H), 1.21 (m, 16H), 0.86 (d, $J_{HH}$ = 6.4 Hz, 3H); $^{13}C$ NMR (75 MHz, $CDCl_3$) δ 186.1, 159.4 (d, $J_{HP}$ = 7.8 Hz), 119.1 (d, $J_{HP}$ = 4.7 Hz), 66.2 (d, $J_{HP}$ = 6.9 Hz), 51.9, 30.5 (d, $J_{CP}$ = 6.0 Hz), 29.7, 29.63, 29.57, 29.4, 29.3, 29.2, 27.0 (d, $J_{CP}$ = 93 Hz) , 25.5, 22.8, 21.2, 21.1, 22.0, 14.2; $^{31}P$ NMR (121 MHz, $CDCl_3$); δ 23.2; HRMS (ESI, $MH^+$) calcd for $C_{19}H_{36}O_5P$ 375.2300, found 375.2296.

**MIC determination.**

The antibacterial activity of the **CyC$_{31yne}$** and **CyC$_{32yne}$** probes as compared to the parent **CyC$_{31}$** and **CyC$_{32}$** against *M. tb* mc²6230 was assessed by determining their MICs in 96-well flat-bottom Nunclon Delta Surface microplates with lid (Thermo-Fisher Scientific, Illkirch, France) using the REMA assay [39, 40]. Briefly, a log-phase *M. tb* mc²6230 culture was diluted to a cell density of $5\times10^6$ cells/mL in 7H9 broth (BD Difco, Le Pont de Claix, France) supplemented with 0.2% glycerol, 0.05% Tween 80 (Sigma-Aldrich, St. Quentin Fallavier, France) and 10% oleic acid, albumin, dextrose, catalase (OADC enrichment; BD Difco) and 24 µg/mL D-panthothenate (Sigma-Aldrich) (7H9-$S^{OADC}$). Then 100 µL of the above inoculum (*i.e.*, $5\times10^5$ cells per well) were added to 100 µL of a serial two-fold dilutions of each **CyC** compound (or DMSO as control) in 7H9-$S^{OADC}$ medium, to a final volume of

200 µL per well of the 96-well plate [16, 33]. Plates were incubated at 37°C for 10-14 days. Then, 20 µL of a 0.025% (*w/v*) resazurin solution was added to each well, and the plates were incubated at 37 °C for color change from blue to pink or violet and for a reading of fluorescence units (FU). Fluorescence corresponding to the resazurin reduction to its metabolite resorufin was quantified using a Tecan Spark 10M multimode microplate reader (Tecan Group Ltd, France) with excitation at 530 nm and emission at 590 nm. MIC values were determined by fitting the relative fluorescence unit (RFU%) sigmoidal dose-response curves in Kaleidagraph 4.2 software (Synergy Software). The lowest drug concentration inhibiting 90% of *M. tb* growth was defined as the $MIC_{90}$. Isoniazid (INH) was used as reference drug.

**Activity-based protein profiling (ABPP) – adapted from [18, 19].**

***Capture of M. tb mc²6230 potential target enzymes from CyC$_{yne}$-treated culture.*** From 1 L of culture at the logarithmic growth stage ($OD_{600}$ ~1.5), *M. tb* mc²6230 cells were harvested by centrifugation at 13,000 rpm for 15 min, and resuspended in 7H9-$S^{OADC}$ at a final theoretical $OD_{600}$ of 40. One mL sample of this homogeneous bacterial suspension was incubated with **CyC$_{31yne}$**, **CyC$_{32yne}$** (500 µM final concentration) or DMSO (control) at 37°C for 4 h under gentle shaking at 75 rpm. Bacteria were harvested (13,000 rpm, 4°C, 15 min) and washed with 3× 500 µL PBS. Cell pellets were resuspended in 750 µL PBS supplemented with EDTA-free protease inhibitors (cOmplete Mini, EDTA-free, Roche) at a 1:1 (*w/v*) ratio. The bacterial cells were then mixed with 350 µL of 0.1 mm diameter glass beads (BioSpec) in a 2-mL Eppendorf tube and disrupted during 2×4 min of violent shaking, with ice cooling between each run, using Mini-Beadbeater-96 (BioSpec). The lysate was cooled down in ice for 5 min and then centrifuged at 4°C and at 1300 rpm for 10 min to remove the cell debris and unbroken cells. The concentration of total proteins in the supernatants was determined *via* the Bradford method, adjusted to a concentration of 1 mg/mL, snap frozen in liquid nitrogen and stored at –80°C until further use.

Both **CyC$_{31yne}$**- and **CyC$_{32yne}$**-treated *M. tb* and DMSO-control lysate samples (500 µL – 0.5 mg total proteins) were subjected to click-chemistry reaction by addition of 8 µL Desthiobiotin-PEG$_3$-N$_3$ (Jena Bioscience, CLK-AZ104P4-100; 40 mM in DMSO), 48.1 µL TBTA ligand (1.667 mM in *t*BuOH/DMSO 8:2 *v/v*) and 20 µL fresh TCEP solution (50 mM in $H_2O$) to the cells. The final concentrations were: 640 µM Desthiobiotin-PEG$_3$-N$_3$, 1.6 mM TCEP and 160 µM TBTA ligand. After gently vortexing of the samples, the cycloaddition reaction was initiated by addition of 16 µL $CuSO_4$ solution (50 mM in $H_2O$ – final concentration: 1.6 mM). The lysates were mixed by vortexing again and incubated for 2 h under gentle rotative agitation (15 rpm) at room temperature in the dark. The proteins were further precipitated overnight at -20°C by adding 4 mL ice-cold acetone, and pelletized by centrifugation (13,000 rpm, 4°C, 15 min). The supernatant was discarded and the proteins were washed with 2×500 µL cold MeOH (resuspension by sonication, 1×10 sec, 10% max. intensity). After centrifugation (13,000 rpm, 4°C, 10 min), the pellets were resuspended in 0.2% (*w/v*) SDS in PBS (250 µL) at room temperature by mild sonication (4×10 sec, 10% max. intensity). Affinity enrichment was performed with 25 µL Pierce™ High Capacity Streptavidin Agarose Resin (Thermo Scientific ref. 20359; pre-washed 3×500 µL 0.4% SDS solution, centrifugation was performed at 5000 rpm for 2 min). Each *M. tb* treated-lysate was enriched for labeled proteins by transfer to the previously washed beads (around 250 µg) and incubated under gentle rotative agitation (15 rpm) at room temperature for 3 h. Beads were stringently washed following pull-down (1 mL each time): 2× 0.4% (*w/v*) SDS in PBS, and 1× 10 M urea in PBS. All centrifugation steps were conducted at 5000 rpm for 2 min at room temperature. The beads containing bound, biotinylated proteins were resuspended in 60 µL PBS buffer pH 7.4 containing 50 mM free D-biotin.

The resulting solution was mixed with 5X Laemmli reducing sample buffer, and heated at 95°C for 5 min. This step allowed the recovery of the captured labelled proteins by exchanging the initially captured Desthiobiotin/streptavidin complex to the greater affinity biotin/streptavidin complex. Each sample was snap frozen in liquid nitrogen and stored at –80°C before mass spectrometry experiments.

To check for unspecific binding, the DMSO-treated lysate sample was also incubated with the streptavidin-agarose beads, and processed as described above.

***Mass spectrometry analysis*.** The protein isolates were loaded on NuPAGE™ 4-12% Bis–tris acrylamide gels according to the manufacturer's instructions (Invitrogen, Life Technologies). Running of samples was stopped as soon as proteins stacked as a single band. Protein containing bands were stained with Thermo Scientific Imperial Blue, cut from the gel, and following reduction and iodoacetamide alkylation, digested with high sequencing grade trypsin (Promega, Madison, WI, USA) [25, 41]. Extracted peptides were concentrated before mass spectrometry analysis. Samples were reconstituted with 0.1% trifluoroacetic acid in 2% acetonitrile and analyzed by liquid chromatography (LC)-tandem MS (MS/MS) using a Q Exactive Plus Hybrid Quadrupole-Orbitrap online with a nanoLC Ultimate 3000 chromatography system (Thermo Fisher Scientific™, San Jose, CA). For each biological sample, 5 µL corresponding to 25% of digested sample were injected in duplicate on the system. After pre-concentration and washing of the sample on a Acclaim PepMap 100 column (C18, 2 cm × 100 µm i.d. 100 Å pore size, 5 µm particle size), peptides were separated on a LC EASY-Spray column (C18, 50 cm × 75 µm i.d., 100 Å, 2 µm, 100 Å particle size) at a flow rate of 300 nL/min with a two-step linear gradient (2-22% acetonitrile/$H_20$; 0.1% formic acid for 100 min and 22-32% acetonitrile/$H_20$; 0.1% formic acid for 20 min). For peptide ionization in the EASY-Spray source, spray voltage was set at 1.9 kV and the capillary temperature at 250 °C. All samples were measured in a data dependent acquisition mode. Each run was preceded by a blank MS run in order to monitor system background. The peptide masses were measured in a survey full scan (scan range 375-1500 m/z, with 70 K FWHM resolution at *m/z*=400, target AGC value of $3.00\times10^6$ and maximum injection time of 100 ms). Following the high-resolution full scan in the Orbitrap, the 10 most intense data-dependent precursor ions were successively fragmented in HCD cell and measured in Orbitrap (normalized collision energy of 25%, activation time of 10 ms, target AGC value of $1.00\times10^5$, intensity threshold $1.00\times10^4$ maximum injection time 100 ms, isolation window 2 *m/z*, 17.5

K FWHM resolution, scan range 200 to 2000 *m/z*). Dynamic exclusion was implemented with a repeat count of 1 and exclusion duration of 20 s.

***Protein identification and quantification.*** Relative intensity-based label-free quantification (LFQ) was processed using the MaxLFQ algorithm [42] from the freely available MaxQuant computational proteomics platform, version 1.6.3.4 [43]. Analysis was done on two biological replicates, each injected two times on mass spectrometers. The acquired raw LC Orbitrap MS data were first processed using the integrated Andromeda search engine [44]. Spectra were searched against the *Mycobacterium Tuberculosis* database extracted from UniProt (date 2021-03-10; 3,993 entries) [45]. The false discovery rate (FDR) at the peptide and protein levels were set to 1% and determined by searching a reverse database. For protein grouping, all proteins that could not be distinguished based on their identified peptides were assembled into a single entry according to the MaxQuant rules. The statistical analysis was done with Perseus program (version 1.6.15) from the MaxQuant environment (www.maxquant.org). Quantifiable proteins were defined as those detected in above 3 of 4 samples in one condition or more. Protein LFQ normalized intensities were base 2 logarithmized to obtain a normal distribution. Missing values were replaced using data imputation by randomly selecting from a normal distribution centred on the lower edge of the intensity values that simulates signals of low abundant proteins using default parameters (a downshift of 1.8 standard deviation and a width of 0.3 of the original distribution). To determine whether a given detected protein was specifically differential, a two-sample *t*-test was done using permutation-based FDR-controlled at 1% and employing 250 permutations. The *p*-value was adjusted using a scaling factor s0 with a value of 1 [46].

The mass spectrometry proteomics data have been deposited to the ProteomeXchange Consortium (www.proteomexchange.org) [47] *via* the PRIDE partner repository [48] with the dataset identifier PXD034921.

**Cloning, expression and purification of HsaD.**

The *rv3569c* gene encoding HsaD was amplified by PCR using *M. tuberculosis* H37Rv genomic DNA and specific forward (*hsaD*-Fwd: 5'-CCAGCATATGACAGCTACCGAGGAATTGACGT-3') and reverse (*hsaD*-Rev: 5'-CCAGAAGCTTTCTGCCACCTCCCAGAAATTCAATC-3') primers. The PCR product was cloned into a pVV16 vector following digestion with NdeI and BamHI restriction sites in 5′ and 3′ ends, respectively, enabling the incorporation of a 6×His-tag in the C-terminus of the HsaD protein. Sequence integrity of the construct was confirmed by DNA sequencing (Eurofins Genomics).

*M. smegmatis* mc²155 electrocompetent cells were prepared as previously described [49], and electroporation procedure was performed as in [16]. Transformants were selected on Middlebrook 7H9 agar plates supplemented with 50 µg/mL hygromycin. Plates were incubated at 37°C for 3 to 5 days. *M. smegmatis* mc²155 carrying *pVV16::hsaD* was cultured in Middlebrook 7H9 broth (BD Difco, Le Pont-de-Claix, France) supplemented with 0.05% (*v/v*) Tween-80, 0.2% (*v/v*) glycerol, 10% (*v/v*) ADS (0.5% albumin, 0.2% dextrose, 0.085% NaCl) and 50 µg/mL hygromycin at 37°C and 220 rpm. When $OD_{600}$ reached 3, bacterial cells were harvested by centrifugation (8,000 ×*g*, 4°C, 1 h), resuspended in lysis buffer (50 mM Tris-HCl, pH 8.0, 1 M NaCl, 0.1% Triton X-100; 30 mL/liter of culture) and disrupted by sonication on ice. After centrifugation, the supernatant was recovered and loaded onto a nickel-chelate affinity resin. The resin was washed with buffer A (50 mM Tris-HCl pH 8, 1 M NaCl, 10 mM imidazole). The protein was eluted with buffer B (50 mM Tris-HCl pH 8, 1 M NaCl, 250 mM imidazole), concentrated and further purified by size-exclusion chromatography on a Superdex 200 16/60 column (GE-Healthcare) equilibrated with buffer C (50 mM Tris-HCl pH 8, 1 M NaCl). Pure fractions of HsaD, as analyzed by SDS-PAGE electrophoresis, were pooled and concentrated to 7.0-7.5 mg/mL using a 10 kDa cut-off ultracentrifugation membrane (Thermoscientific). HsaD was stored at –80°C. Theoretical physical properties (molecular mass, extinction coefficient at 280 nm, and isoelectric point) of HsaD containing the 6×His tag at the C-terminal position were computed with the ProtParam tool [50] (http://ca.expasy.org/tools/protparam.htmL).

**Inhibition assays.**

The lipase-inhibitor pre-incubation method was used to test, in aqueous medium and in the absence of substrate, the possible direct reactions between the enzyme and the **CyC** inhibitors as already reported [32, 34]. Briefly, each inhibitor was incubated overnight at 23°C with HsaD (12 µM final concentration in 50 mM Tris-HCl buffer pH 8, 67 mM NaCl) at varying inhibitor molar excess ($x_I$) [32] ranging from 0.2 to 80 related to 1 mol of enzyme, in a final volume of 100 µL. After the incubation period, the residual HsaD activity was measured *via* monitoring the degradation of the synthetic substrate HOPDA (200 µM final concentration) at $OD_{450nm}$ using a microtiter plate scanning spectrophotometer (PowerWave™, Bio-Tek Instruments) as described in [21].The variation in the residual enzyme activity allowed the determination of the inhibitor molar excess that reduces the enzyme activity to 50% of its initial value ($x_{I50}$) [32, 34]. Dose response curves were fitted using Kaleidagraph *v*.4.03 (Synergy Software). Results are expressed as mean values ± SD of two independent assays.

**Mass-spectrometry analysis of HsaD-CyC complexes.**

***Intact protein mass analysis*.** Protein masses were determined on purified solution samples. To this end, the proteins in 10 µL of 50mM Tris pH 8, 100 mM NaCl buffer were desalted on ZipTip C4 (Millipore) and eluted by 3 µL of sinapinic acid matrix solution in 0.3% TFA/$CH_3CN$ (50:50 *v/v*). One µL of the mix was spotted on the target and analyzed by MALDI-TOF on an Ultraflex III spectrometer (Bruker Daltonics, Wissembourg, France) controlled by the Flexcontrol 3.0 package (Build 51) and operated in the linear mode, using a maximum accelerating potential of 25 kV and a 20000-100000 *m/z* range (LP_66kDa method). The laser frequency was fixed to 100 Hz and ~1000 shots per sample were cumulated. Four external standards (Protein Calibration Standard II, Bruker Daltonics) were used to calibrate each spectrum to a mass accuracy within 100 ppm. Peak picking was performed using the FlexAnalysis 3.0 software with an adapted analysis method. Parameters

used were: centroid peak detection algorithm, S/N threshold fixed to 5 and a quality factor threshold of 30.

***Peptide mass fingerprinting.*** Proteins in SDS-PAGE gel-excised bands were submitted to trypsin digestion using a slightly modified Shevchenko protocol [41]. Briefly, the bands were washed and destained using 100 mM $NH_4HCO_3$ (pH 8.0), reduced using DTT 10 mM (56°C, 45 min) and alkylated with 55 mM iodoacetamide (25°C, 30 min in the dark), both in 100 mM $NH_4HCO_3$ (pH 8.0), dried at room temperature, and reswollen into 25 mM $NH_4HCO_3$ supplemented with 12.5 ng/µL trypsin (V5111, Promega) overnight at 37°C. Peptide extracts collected from the digestion solution, from a first extract by sonication in 5% formic acid, and from a second one in 5% formic acid / $CH_3CN$ (40:60 *v/v*) were pooled and dried in a centrifugal vacuum system.

Peptides were then resuspended in a α-cyano-4-hydroxycinnamic acid matrix solution (saturated solution in 50% acetonitrile / 0.3% TFA), and 1 µL was spotted on the Maldi metal target. Mass analyses were performed on a MALDI-TOF-TOF Ultraflex III spectrometer (Bruker Daltonics, Wissembourg, France) controlled by the Flexcontrol 3.0 package (Build 51). This instrument was used at a maximum accelerating potential of 25 kV and was operated in reflector mode and the *m/z* range from 600 to 3500. Six external standards (Peptide Calibration Standard II, Bruker Daltonics) were used to calibrate each spectrum to a mass accuracy within 10 ppm with a minimal resolution of 10000 for the angiotensin II peak (Monoisotopic mass = 1046,542 Da). Peak picking was performed with FlexAnalysis 3.0 software (Bruker) with an adapted analysis method. Parameters used were as follows: SNAP peak detection algorithm, S/N threshold fixed to 6 and a quality factor threshold of 30. The peaks obtained were then compared to the theoretical digestion peaks list of the total protein with Biotools software.

***MS/MS analyses.*** Sequences of modified peptides were confirmed by MS/MS analyses on the Maldi TOF-TOF Ultraflex III spectrometer (Bruker Daltonics, Wissembourg, France) using the LIFT_2017 method after calibration. LIFT mass spectra were acquired in the positive ion mode. Metastable fragmentation was induced by a nitrogen laser (337 nm) without the further use of collision gas.

Precursor ions were accelerated to 8 kV and selected in a timed ion gate. In the LIFT-cell the fragments were further accelerated to 19.07 kV. The reflector potential was 29.6 kV [51].

**Crystallization, data collection and processing.**

Crystallization trials on the native form of HsaD were performed by the sitting-drop vapor-diffusion method using a TECAN EVO pipetting robot to fill Greiner plates with commercial screens and a Mosquito® (TTP labtech) crystallization robot to dispense the protein and reservoir solutions. Crystal hits emerged from a condition of the AmSO4 suite (NeXtal) containing 2 M $(NH_4)_2SO_4$, 0.1 M MES-Na pH 6.5 and 5% (*v/v*) PEG400 and after several optimization rounds well diffracting crystals were obtained by the hanging-drop vapor-diffusion method in Linbro plates by mixing 1 µL protein solution at 7.5 mg/mL with 0.5 µL reservoir solution composed of 1.5 to 1.7 M $(NH_4)_2SO_4$, 0.1 M MES-Na pH 6.5 and 5 to 10% (*v/v*) PEG400.

To obtain the structure of HsaD in complex with the **CyC** inhibitors, the protein at 7.5 mg/mL was mixed either with each of the **CyC$_{7\beta}$**, **CyC$_{8\beta}$** and **CyC$_{17}$** inhibitors dissolved in Transcutol® HP (Gattefossé SAS) at a molar excess $x_I = 100$ and incubated at room temperature for 2 h, or with **CyC$_{31}$** dissolved in DMSO at a molar excess $x_I = 2.5$ and incubated at room temperature for 24 h.

Crystallization of HsaD in complex with the **CyC** inhibitors was performed as outlined above for the native form of HsaD. Crystals of native HsaD, and HsaD in complex with the **CyC** inhibitors were cryo-protected with reservoir solution supplemented with 30% (*v/v*) glycerol prior flash-freezing in liquid nitrogen. X-ray diffraction data were acquired at beam lines Proxima1 and Proxima2a at the Synchrotron Soleil, Gif-sur-Yvette. Diffraction data were processed with XDS [52] and scaled and merged using the CCP4 suite [53, 54] of programs Pointless [55], AimLess [56] and Truncate [57].

The structure of native HsaD was solved by molecular replacement with the program Phaser [58] using the structural coordinates of the same protein (PDB: 2VF2 – 2.35 Å resolution [35], 100% sequence identity) as the search model. The complex HsaD-**CyC** structures were solved by molecular replacement using the coordinates of native HsaD as the search model. Refinement and model

adjustment were carried out with the programs Refmac [59] and Coot [60], respectively. Random sets of ~5% of reflections, depending on the resolution limit, were set-aside for cross-validation purposes. The composition of cross-validation data sets was systematically taken over from the parent data set, except for the complex HsaD-**CyC**$_{7\beta}$, which belongs to a different space group. The covalent link between the **CyC** ligands and the catalytic serine $S^{114}$, and stereochemical restraints for the inhibitors, were generated by JLigand [61]. Model quality was assessed with internal modules of Coot [60] and with the Molprobity server [62]. Ligands were fitted into unbiased Fo–Fc difference electron density maps calculated after 5-7 cycles of restrained refinement with Refmac [59]. Figures representing structural renderings were generated with the PyMOL Molecular Graphics System (Version 2, Schrödinger, LLC).

**In silico molecular docking experiments.**

Autodock Vina [36] was used as previously reported [16, 20, 63] to generate the putative binding modes of the various **CyC** inhibitors into the active site of HsaD. The PyMOL Molecular Graphics System (version 1.4, Schrödinger, LLC) was used as the working environment with an in-house version of the AutoDock/Vina PyMOL plugin [63]. The X-ray crystallographic structure of HsaD in complex with the **CyC**$_{31}$ inhibitor (PDB: 7ZM4) was used as the receptor. Docking runs were performed after removing the bound **CyC**$_{31}$ from the enzyme active site, and replacing the catalytic $Ser^{114}$ with a glycine residue to enable the ligand (*i.e.*, the inhibitor) to adopt a suitable position corresponding to the pre-bound intermediate before the nucleophilic attack in the enzyme active site. The box size used was chosen to fit the whole enzyme's active site cleft and allowed non-constructive binding positions. The three-dimensional structures of the **CyC** compounds were constructed using Chem3D Ultra 11.0 software, and their geometry was refined using the Avogadro open-source molecular builder and visualization tool (version 1.2.0. http://avogadro.cc/) [64].

## ACKNOWLEDGEMENTS

This work was supported by the CNRS, Aix Marseille University, and the Agence Nationale de la Recherche (grant N°ANR-19-CE44-0011) and by the French Infrastructure for Integrated Structural Biology (FRISBI) (grant N°ANR-10-INSB-05-01). Proteomics analyses were done using the mass spectrometry facility of Marseille Proteomics (marseille-proteomique.univ-amu.fr) supported by IBISA, the Cancéropôle PACA, the Provence-Alpes-Côte d'Azur Région, the Institut Paoli-Calmettes, and Fonds Europeen de Développement Régional (FEDER). We thank Synchrotron Soleil for beamtime allocation and beam line staff for assistance with data collection. The synthetic substrate HOPDA was kindly provided to us by Prof. Edith Sim (Oxford University) and Dr Ali Ryan (Northumbria University).

## DATA ACCESSIBILITY

The atomic coordinates and structure factors (PDB: 7ZJT, 7ZM1, 7ZM2, 7ZM3 and 7ZM4) have been deposited in the Protein Data Bank (https://www.wwpdb.org/).

## AUTHOR CONTRIBUTIONS

S.B., G.S. and J.-F.C. conceptualization; S.B., P.F., S.A., L.C. and G.S. data curation; S.B., R.A., P.F., V.R-Z., I.P., V.P., S.A. and L.C. investigation; S.B., R.A., P.F., V.R-Z., I.P., V.P., S.A. and L.C. methodology; G.R.G. and C.D.S. resources; S.B., R.A., C.D.S., S.C., G.S. and J.-F.C. formal analysis; S.B., R.A., P.F. and J.-F.C. visualization; S.B. and J.-F.C. writing-original draft; S.B., Y.B., C.D.S., P.F., S.C., L.C., G.S. and J.-F.C. writing-review and editing. G.S. and J.-F.C. supervision; J.-F.C. funding acquisition; J.-F.C. validation; J.-F.C. project administration. All authors have given approval to the final version of the manuscript.

**REFERENCES**


1. WHO (2021) Global tuberculosis report, https://www.who.int/teams/global-tuberculosis-programme/data.

2. Mallick, I., Santucci, P., Poncin, I., Point, V., Kremer, L., Cavalier, J. F. & Canaan, S. (2021) Intrabacterial lipid inclusions in mycobacteria: unexpected key players in survival and pathogenesis?, *FEMS Microbiol Rev.* **45**, fuab029.

3. Rengarajan, J., Bloom, B. R. & Rubin, E. J. (2005) Genome-wide requirements for *Mycobacterium tuberculosis* adaptation and survival in macrophages, *Proc Natl Acad Sci U S A.* **102**, 8327-8332.

4. Sassetti, C. M. & Rubin, E. J. (2003) Genetic requirements for mycobacterial survival during infection, *Proc Natl Acad Sci U S A.* **100**, 12989-94.

5. Pandey, A. K. & Sassetti, C. M. (2008) Mycobacterial persistence requires the utilization of host cholesterol, *Proc Natl Acad Sci U S A.* **105**, 4376-80.

6. Ouellet, H., Johnston, J. B. & de Montellano, P. R. (2011) Cholesterol catabolism as a therapeutic target in *Mycobacterium tuberculosis*, *Trends Microbiol.* **19**, 530-9.

7. Lovewell, R. R., Sassetti, C. M. & VanderVen, B. C. (2016) Chewing the fat: lipid metabolism and homeostasis during *M. tuberculosis* infection, *Curr Opin Microbiol.* **29**, 30-6.

8. Van der Geize, R., Yam, K., Heuser, T., Wilbrink, M. H., Hara, H., Anderton, M. C., Sim, E., Dijkhuizen, L., Davies, J. E., Mohn, W. W. & Eltis, L. D. (2007) A gene cluster encoding cholesterol catabolism in a soil actinomycete provides insight into *Mycobacterium tuberculosis* survival in macrophages, *Proc Natl Acad Sci U S A.* **104**, 1947-1952.

9. Griffin, J. E., Gawronski, J. D., Dejesus, M. A., Ioerger, T. R., Akerley, B. J. & Sassetti, C. M. (2011) High-resolution phenotypic profiling defines genes essential for mycobacterial growth and cholesterol catabolism, *PLoS Pathog.* **7**, e1002251.

10. Singh, G., Singh, G., Jadeja, D. & Kaur, J. (2010) Lipid hydrolizing enzymes in virulence: *Mycobacterium tuberculosis* as a model system, *Crit Rev Microbiol.* **36**, 259-69.

11. Johnson, G. (2017) The alpha/beta Hydrolase Fold Proteins of *Mycobacterium tuberculosis*, with Reference to their Contribution to Virulence, *Current protein & peptide science.* **18**, 190-210.

12. Dedieu, L., Serveau-Avesque, C., Kremer, L. & Canaan, S. (2013) Mycobacterial lipolytic enzymes: A gold mine for tuberculosis research, *Biochimie.* **95**, 66-73.

13. Keller, L. J., Babin, B. M., Lakemeyer, M. & Bogyo, M. (2019) Activity-based protein profiling in bacteria: Applications for identification of therapeutic targets and characterization of microbial communities, *Curr Opin Chem Biol.* **54**, 45-53.

14. Spilling, C. D. (2019) The Chemistry and Biology of Cyclophostin, the Cyclipostins and Related Compounds, *Molecules.* **24**.

15. Cavalier, J. F., Spilling, C. D., Durand, T., Camoin, L. & Canaan, S. (2021) Lipolytic enzymes inhibitors: A new way for antibacterial drugs discovery, *Eur J Med Chem.* **209**, 112908.
16. Nguyen, P. C., Delorme, V., Bénarouche, A., Martin, B. P., Paudel, R., Gnawali, G. R., Madani, A., Puppo, R., Landry, V., Kremer, L., Brodin, P., Spilling, C. D., Cavalier, J.-F. & Canaan, S. (2017) Cyclipostins and Cyclophostin analogs as promising compounds in the fight against tuberculosis, *Scientific Reports.* **7**, 11751.
17. Cravatt, B. F., Wright, A. T. & Kozarich, J. W. (2008) Activity-based protein profiling: from enzyme chemistry to proteomic chemistry, *Annu Rev Biochem.* **77**, 383-414.
18. Krysiak, J. & Sieber, S. A. (2017) Activity-Based Protein Profiling in Bacteria in *Activity-Based Proteomics: Methods and Protocols* (Overkleeft, H. S. & Florea, B. I., eds) pp. 57-74, Springer New York, New York, NY.
19. Lehmann, J., Cheng, T. Y., Aggarwal, A., Park, A. S., Zeiler, E., Raju, R. M., Akopian, T., Kandror, O., Sacchettini, J. C., Moody, D. B., Rubin, E. J. & Sieber, S. A. (2018) An Antibacterial beta-Lactone Kills *Mycobacterium tuberculosis* by Disrupting Mycolic Acid Biosynthesis, *Angew Chem Int Ed Engl.* **57**, 348-353.
20. Li, M., Patel, H. V., Cognetta, A. B., Smith, T. C., Mallick, I., Cavalier, J.-F., Previti, M. L., Canaan, S., Aldridge, B. B., Cravatt, B. F. & Seeliger, J. C. (2022) Identification of cell wall synthesis inhibitors active against *Mycobacterium tuberculosis* by competitive activity-based protein profiling, *Cell Chem Biol.* **29**, 883-896.e5.
21. Ryan, A., Polycarpou, E., Lack, N. A., Evangelopoulos, D., Sieg, C., Halman, A., Bhakta, S., Eleftheriadou, O., McHugh, T. D., Keany, S., Lowe, E. D., Ballet, R., Abuhammad, A., Jacobs, W. R., Jr., Ciulli, A. & Sim, E. (2017) Investigation of the mycobacterial enzyme HsaD as a potential novel target for anti-tubercular agents using a fragment-based drug design approach, *Br J Pharmacol.* **174**, 2209-2224.
22. Dutta, S., Malla, R. K., Bandyopadhyay, S., Spilling, C. D. & Dupureur, C. M. (2010) Synthesis and kinetic analysis of some phosphonate analogs of cyclophostin as inhibitors of human acetylcholinesterase, *Bioorg Med Chem.* **18**, 2265-74.
23. Vasilieva, E., Dutta, S., Malla, R. K., Martin, B. P., Spilling, C. D. & Dupureur, C. M. (2015) Rat hormone sensitive lipase inhibition by cyclipostins and their analogs, *Bioorg Med Chem.* **23**, 944-952.
24. Neef, A. B. & Schultz, C. (2009) Selective fluorescence labeling of lipids in living cells, *Angew Chem Int Ed Engl.* **48**, 1498-500.
25. Madani, A., Ridenour, J. N., Martin, B. P., Paudel, R. R., Abdul Basir, A., Le Moigne, V., Herrmann, J. L., Audebert, S., Camoin, L., Kremer, L., Spilling, C. D., Canaan, S. & Cavalier, J. F.

(2019) Cyclipostins and Cyclophostin Analogues as Multitarget Inhibitors That Impair Growth of *Mycobacterium abscessus*, *ACS Infect Dis.* **5**, 1597-1608.

26. Nguyen, P. C., Madani, A., Santucci, P., Martin, B. P., Paudel, R. R., Delattre, S., Herrmann, J.-L., Spilling, C. D., Kremer, L., Canaan, S. & Cavalier, J.-F. (2018) Cyclophostin and Cyclipostins analogs, new promising molecules to treat mycobacterial-related diseases, *Int J Antimicrob Agents.* **51**, 651-654.

27. Niphakis, M. J. & Cravatt, B. F. (2014) Enzyme inhibitor discovery by activity-based protein profiling, *Annu Rev Biochem.* **83**, 341-77.

28. Díez-González, S. (2016) Chapter Three - Copper(I)–Acetylides: Access, Structure, and Relevance in Catalysis in *Advances in Organometallic Chemistry* (Pérez, P. J., ed) pp. 93-141, Academic Press.

29. Lack, N. A., Kawamura, A., Fullam, E., Laurieri, N., Beard, S., Russell, A. J., Evangelopoulos, D., Westwood, I. & Sim, E. (2009) Temperature stability of proteins essential for the intracellular survival of *Mycobacterium tuberculosis*, *Biochem J.* **418**, 369-78.

30. Lack, N. A., Yam, K. C., Lowe, E. D., Horsman, G. P., Owen, R. L., Sim, E. & Eltis, L. D. (2010) Characterization of a carbon-carbon hydrolase from *Mycobacterium tuberculosis* involved in cholesterol metabolism, *J Biol Chem.* **285**, 434-43.

31. Nguyen, P. C., Delorme, V., Benarouche, A., Guy, A., Landry, V., Audebert, S., Pophillat, M., Camoin, L., Crauste, C., Galano, J. M., Durand, T., Brodin, P., Canaan, S. & Cavalier, J. F. (2018) Oxadiazolone derivatives, new promising multi-target inhibitors against *M. tuberculosis*, *Bioorg Chem.* **81**, 414-424.

32. Point, V., Malla, R. K., Diomande, S., Martin, B. P., Delorme, V., Carriere, F., Canaan, S., Rath, N. P., Spilling, C. D. & Cavalier, J.-F. (2012) Synthesis and kinetic evaluation of Cyclophostin and Cyclipostins phosphonate analogs as selective and potent inhibitors of microbial lipases, *J Med Chem.* **55**, 10204-10219.

33. Nguyen, P. C., Nguyen, V. S., Martin, B. P., Fourquet, P., Camoin, L., Spilling, C. D., Cavalier, J.-F., Cambillau, C. & Canaan, S. (2018) Biochemical and structural characterization of TesA, a major thioesterase required for outer-envelope lipid biosynthesis in *M. tuberculosis*, *J Mol Biol.* **430**, 5120-5136.

34. Viljoen, A., Richard, M., Nguyen, P. C., Fourquet, P., Camoin, L., Paudal, R. R., Gnawali, G. R., Spilling, C. D., Cavalier, J.-F., Canaan, S., Blaise, M. & Kremer, L. (2018) Cyclipostins and Cyclophostin analogs inhibit the antigen 85C from *Mycobacterium tuberculosis* both *in vitro* and *in vivo*, *J Biol Chem.* **293**, 2755–2769.

35. Lack, N., Lowe, E. D., Liu, J., Eltis, L. D., Noble, M. E. M., Sim, E. & Westwood, I. M. (2008) Structure of HsaD, a steroid-degrading hydrolase, from *Mycobacterium tuberculosis*, *Acta Crystallographica Section F.* **64**, 2-7.

36. Trott, O. & Olson, A. J. (2010) AutoDock Vina: Improving the speed and accuracy of docking with a new scoring function, efficient optimization, and multithreading, *Journal of Computational Chemistry.* **31**, 455-461.

37. Babin, B. M., Keller, L. J., Pinto, Y., Li, V. L., Eneim, A. S., Vance, S. E., Terrell, S. M., Bhatt, A. S., Long, J. Z. & Bogyo, M. (2022) Identification of covalent inhibitors that disrupt *M. tuberculosis* growth by targeting multiple serine hydrolases involved in lipid metabolism, *Cell Chem Biol.* **29**, 897-909 e7.

38. Rohde, K. H., Abramovitch, R. B. & Russell, D. G. (2007) *Mycobacterium tuberculosis* invasion of macrophages: linking bacterial gene expression to environmental cues, *Cell Host Microbe.* **2**, 352-64.

39. Palomino, J. C., Martin, A., Camacho, M., Guerra, H., Swings, J. & Portaels, F. (2002) Resazurin microtiter assay plate: simple and inexpensive method for detection of drug resistance in *Mycobacterium tuberculosis*, *Antimicrob Agents Chemother.* **46**, 2720-2722.

40. Rybniker, J., Vocat, A., Sala, C., Busso, P., Pojer, F., Benjak, A. & Cole, S. T. (2015) Lansoprazole is an antituberculous prodrug targeting cytochrome bc1, *Nat Commun.* **6**, 7659.

41. Shevchenko, A., Wilm, M., Vorm, O. & Mann, M. (1996) Mass spectrometric sequencing of proteins silver-stained polyacrylamide gels, *Analytical chemistry.* **68**, 850-8.

42. Cox, J., Hein, M. Y., Luber, C. A., Paron, I., Nagaraj, N. & Mann, M. (2014) Accurate proteome-wide label-free quantification by delayed normalization and maximal peptide ratio extraction, termed MaxLFQ, *Mol Cell Proteomics.* **13**, 2513-2526.

43. Cox, J. & Mann, M. (2008) MaxQuant enables high peptide identification rates, individualized p.p.b.-range mass accuracies and proteome-wide protein quantification, *Nat Biotechnol.* **26**, 1367-1372.

44. Cox, J., Neuhauser, N., Michalski, A., Scheltema, R. A., Olsen, J. V. & Mann, M. (2011) Andromeda: a peptide search engine integrated into the MaxQuant environment, *J Proteome Res.* **10**, 1794-1805.

45. The UniProt, C. (2017) UniProt: the universal protein knowledgebase, *Nucleic Acids Res.* **45**, D158-D169.

46. Tusher, V. G., Tibshirani, R. & Chu, G. (2001) Significance analysis of microarrays applied to the ionizing radiation response, *Proc Natl Acad Sci U S A.* **98**, 5116-5121.

47. Deutsch, E. W., Bandeira, N., Sharma, V., Perez-Riverol, Y., Carver, J. J., Kundu, D. J., Garcia-Seisdedos, D., Jarnuczak, A. F., Hewapathirana, S., Pullman, B. S., Wertz, J., Sun, Z., Kawano, S.,

Okuda, S., Watanabe, Y., Hermjakob, H., MacLean, B., MacCoss, M. J., Zhu, Y., Ishihama, Y. & Vizcaino, J. A. (2020) The ProteomeXchange consortium in 2020: enabling 'big data' approaches in proteomics, *Nucleic Acids Res.* **48**, D1145-D1152.

48. Perez-Riverol, Y., Bai, J., Bandla, C., Garcia-Seisdedos, D., Hewapathirana, S., Kamatchinathan, S., Kundu, D. J., Prakash, A., Frericks-Zipper, A., Eisenacher, M., Walzer, M., Wang, S., Brazma, A. & Vizcaino, J. A. (2022) The PRIDE database resources in 2022: a hub for mass spectrometry-based proteomics evidences, *Nucleic Acids Res.* **50**, D543-D552.

49. Goude, R., Roberts, D. M. & Parish, T. (2015) Electroporation of Mycobacteria in *Mycobacteria Protocols* (Parish, T. & Roberts, D. M., eds) pp. 117-130, Springer New York, New York, NY.

50. Gasteiger, E., Hoogland, C., Gattiker, A., Duvaud, S. e., Wilkins, M. R., Appel, R. D. & Bairoch, A. (2005) Protein Identification and Analysis Tools on the ExPASy Server in *The Proteomics Protocols Handbook* (Walker, J. M., ed) pp. 571-607, Humana Press, Totowa, NJ.

51. Suckau, D., Resemann, A., Schuerenberg, M., Hufnagel, P., Franzen, J. & Holle, A. (2003) A novel MALDI LIFT-TOF/TOF mass spectrometer for proteomics, *Analytical and bioanalytical chemistry.* **376**, 952-65.

52. Kabsch, W. (2010) Integration, scaling, space-group assignment and post-refinement, *Acta Crystallographica Section D.* **66**, 133-144.

53. Potterton, E., Briggs, P., Turkenburg, M. & Dodson, E. (2003) A graphical user interface to the CCP4 program suite, *Acta Crystallogr D Biol Crystallogr.* **59**, 1131-7.

54. Winn, M. D., Ballard, C. C., Cowtan, K. D., Dodson, E. J., Emsley, P., Evans, P. R., Keegan, R. M., Krissinel, E. B., Leslie, A. G., McCoy, A., McNicholas, S. J., Murshudov, G. N., Pannu, N. S., Potterton, E. A., Powell, H. R., Read, R. J., Vagin, A. & Wilson, K. S. (2011) Overview of the CCP4 suite and current developments, *Acta Crystallogr D Biol Crystallogr.* **67**, 235-42.

55. Evans, P. R. (2011) An introduction to data reduction: space-group determination, scaling and intensity statistics, *Acta Crystallogr D Biol Crystallogr.* **67**, 282-92.

56. Evans, P. R. & Murshudov, G. N. (2013) How good are my data and what is the resolution?, *Acta Crystallographica Section D.* **69**, 1204-1214.

57. French, S. & Wilson, K. (1978) On the treatment of negative intensity observations, *Acta Crystallographica Section A.* **34**, 517-525.

58. McCoy, A. J., Grosse-Kunstleve, R. W., Adams, P. D., Winn, M. D., Storoni, L. C. & Read, R. J. (2007) Phaser crystallographic software, *Journal of applied crystallography.* **40**, 658-674.

59. Murshudov, G. N., Skubák, P., Lebedev, A. A., Pannu, N. S., Steiner, R. A., Nicholls, R. A., Winn, M. D., Long, F. & Vagin, A. A. (2011) REFMAC5 for the refinement of macromolecular crystal structures, *Acta Crystallogr D Biol Crystallogr.* **67**, 355-67.

60. Emsley, P. & Cowtan, K. (2004) Coot: model-building tools for molecular graphics, *Acta Crystallographica Section D: Biological Crystallography.* **60**, 2126-2132.

61. Lebedev, A. A., Young, P., Isupov, M. N., Moroz, O. V., Vagin, A. A. & Murshudov, G. N. (2012) JLigand: a graphical tool for the CCP4 template-restraint library, *Acta Crystallogr D Biol Crystallogr.* **68**, 431-40.

62. Williams, C. J., Headd, J. J., Moriarty, N. W., Prisant, M. G., Videau, L. L., Deis, L. N., Verma, V., Keedy, D. A., Hintze, B. J., Chen, V. B., Jain, S., Lewis, S. M., Arendall, W. B., 3rd, Snoeyink, J., Adams, P. D., Lovell, S. C., Richardson, J. S. & Richardson, D. C. (2018) MolProbity: More and better reference data for improved all-atom structure validation, *Protein science : a publication of the Protein Society.* **27**, 293-315.

63. Seeliger, D. & de Groot, B. L. (2010) Ligand docking and binding site analysis with PyMOL and Autodock/Vina, *J Comput Aided Mol Des.* **24**, 417-22.

64. Hanwell, M. D., Curtis, D. E., Lonie, D. C., Vandermeersch, T., Zurek, E. & Hutchison, G. R. (2012) Avogadro: an advanced semantic chemical editor, visualization, and analysis platform, *J Cheminform.* **4**, 17.

65. Kapopoulou, A., Lew, J. M. & Cole, S. T. (2011) The MycoBrowser portal: a comprehensive and manually annotated resource for mycobacterial genomes, *Tuberculosis (Edinb).* **91**, 8-13.

**SUPPORTING INFORMATION**

**Table S1. CyC$_{31yne}$** target proteins identified in *M. tb* mc²6230 culture through CC-ABPP by LC-ESI-MS/MS analysis. Only positive hits with a *p*-value <0.01 and a fold-change ≥1.2 are reported

**Table S2. CyC$_{32yne}$** target proteins identified in *M. tb* mc²6230 culture through CC-ABPP by LC-ESI-MS/MS analysis. Only positive hits with a *p*-value <0.01 and a fold-change ≥1.2 are reported

**Table S3.** Proteins differentially captured with **CyC$_{31yne}$** and **CyC$_{32yne}$** at a *p*-value ≤ 0.01 and a fold-change ≥ 1.2

**Fig. S1.** $^{1}$H, $^{13}$C and $^{31}$P NMR spectra of the **CyC$_{31}$**, **CyC$_{32}$**, **CyC$_{31yne}$** and **CyC$_{32yne}$** compounds

## TABLES

**Table 1.** Data collection and refinement statistics (molecular replacement). Values in parentheses are for the highest-resolution shell.

| | **Native HsaD** | **HsaD-CyC$_{7\beta}$** | **HsaD-CyC$_{8\beta}$** | **HsaD-CyC$_{17}$** | **HsaD-CyC$_{31}$** |
|---|---|---|---|---|---|
| ***Data collection*** | | | | | |
| Space group | $P222_1$ | $P2_12_12$ | $P222_1$ | $P222_1$ | $P222_1$ |
| Cell dimensions a, b, c (Å) | 76.8 87.4 106.2 | 76.9 78.4 92.0 | 76.8 87.2 105.9 | 77.0 87.4 106.1 | 76.7 87.2 105.6 |
| Resolution (Å) | 45.38 - 1.96 (2.01 - 1.96) | 47.14 - 2.15 (2.22 - 2.15) | 45.26 - 2.20 (2.27 - 2.20) | 45.36 - 1.81 (1.85 - 1.81) | 45.21 - 1.62 (1.64 - 1.62) |
| No. reflections | 51930 (3434) | 30915 (2594) | 36843 (3132) | 66020 (3704) | 91211 (4202) |
| $R_{merge}$ | 0.148 (1.165) | 0.158 (0.996) | 0.157 (1.349) | 0.118 (1.390) | 0.081 (1.466) |
| $R_{pim}$ | 0.047 (0.378) | 0.058 (0.373) | 0.048 (0.413) | 0.033 (0.404) | 0.023 (0.424) |
| CC (1/2) | 0.998 (0.653) | 0.996 (0.769) | 0.998 (0.696) | 0.999 (0.638) | 0.999 (0.738) |
| $I/\sigma_I$ | 13.8 (2.1) | 11.7 (2.4) | 12.4 (2.4) | 16.5 (2.0) | 17.2 (1.9) |
| Completeness (%) | 99.6 (94.4) | 99.8 (98.5) | 100.0 (99.8) | 99.8 (96.0) | 99.7 (94.7) |
| Multiplicity | 10.5 (9.9) | 8.1 (7.8) | 11.4 (11.4) | 13.4 (12.4) | 13.5 (12.3) |
| Wilson B ($Å^2$) | 14.8 | 17.4 | 30.4 | 19.1 | 19.6 |
| ***Refinement*** | | | | | |
| $R_{work}$ (%) | 18.31 | 18.14 | 17.54 | 18.23 | 18.36 |
| $R_{free}$ (%) | 21.89 | 21.18 | 22.36 | 21.32 | 20.22 |
| *No. atoms* | | | | | |
| protein | 4388 | 4388 | 4388 | 4388 | 4388 |
| ligand / ions | 11 | 75 | 35 | 20 | 35 |
| water | 293 | 125 | 108 | 336 | 377 |
| *R.m.s. deviations* | | | | | |
| Bond lengths (Å) | 0.0099 | 0.0133 | 0.0139 | 0.0087 | 0.0067 |
| Bond angles (°) | 1.5555 | 1.7584 | 1.8079 | 1.5172 | 1.3682 |
| *Ramachandran* | | | | | |
| Favored (%) | 96.99 | 95.74 | 96.45 | 97.87 | 98.05 |
| Outliers (%) | 0 | 0 | 0 | 0 | 0 |
| PDB Code | 7ZJT | 7ZM1 | 7ZM2 | 7ZM3 | 7ZM4 |

## FIGURE LEGENDS

**Fig. 1**. **Click chemistry activity-based protein profiling on a *M. tb* living culture. (A) *Synthesis of the monocyclic phosphate $CyC_{31}$ and phosphonate $CyC_{32}$, as well as the corresponding alkyne derivatives $CyC_{31yne}$ and $CyC_{32yne}$.*** The inserted table depicts the antibacterial activity of the four **CyC** derivatives against *M. tb* $mc^2$6230 growth in broth medium, reported as $MIC_{90}$. Values are mean of at least two independent assays performed in triplicate. INH, isoniazid used as control drug. **(B) *Click chemistry activity-based protein profiling (CC-ABPP) typical workflow for the identification of proteins covalently bound to $CyC_{yne}$ inhibitors***. Exponential growth phase culture of *M. tb* $mc^2$6230 was pre-treated with either $CyC_{31yne}$ or $CyC_{32yne}$ prior to cell lysis and subsequent click-reaction with Azide-$PEG_3$-Desthiobiotin reporter. Samples were then treated with streptavidin-agarose beads for the capture and enrichment of labeled proteins, followed by tryptic digestion. Tandem mass spectrometry analyses and subsequent differential peptides analysis allowed the identification of the **CyC** target enzymes. **(C) *Proteomics analysis of CC-ABPP applied to a M. tb $mc^2$6230 culture.* a) Volcano plot of the proteomic analysis of $CyC_{31yne}$** showing the significance of two sample *t*-test (-Log(*p*-value)) *versus* fold-change ($Log_2$(LFQ normalized intensity in $CyC_{31yne}$ *vs*. non-specific condition)) on the *y* and *x* axes, respectively. Only proteins identified with a score threshold value ≥ 60 were considered. Here the plot is zoomed on the positive difference between the two conditions. The dashed lines indicate the threshold of *p-value* ≤ 0.01 and a fold-change ≥ 1.2. The two insets show the proteins already identified *via* competitive ABPP with **$CyC_{17}$** [16]. **b) Venn diagram** showing the total number of proteins differentially captured with **$CyC_{31yne}$** and **$CyC_{32yne}$** at a *p-value* ≤ 0.01 and a fold-change ≥ 1.2. **c) Functional categories** of *M. tb* proteins identified with **$CyC_{31yne}$** and **$CyC_{32yne}$**, respectively, according to the functional classification system of the Mycobrowser database [65]. The numbers correspond to the total number of identified proteins in each category. Proteins without functional annotation are denoted as uncharacterized proteins.

**Fig. 2. Covalent binding to HsaD and inhibition by CyC compounds. (A) *HsaD purification*.** Mw, standard from Euromedex; purified HsaD, 2.3 µg loaded. **(B) *Chemical structures*** of **$CyC_{7β}$** and **$CyC_{8β}$**, *cis*-monocyclic enol phosphonate analogs of Cyclophostin, and **$CyC_{17}$**, **$CyC_{31}$** and **$CyC_{32}$**, monocyclic enol phosphate analogs of Cyclipostins. **(C) *Inhibition of the HsaD MCP hydrolase activity is mediated by the covalent binding of CyC analogs***. Dose-response curves for **$CyC_{7β}$**, **$CyC_{8β}$**, **$CyC_{17}$**, **$CyC_{31}$** and **$CyC_{32}$** showing the decrease in HsaD enzymatic activity on the HOPDA substrate, with the calculated $x_{I50}$ values. **(D) *Global mass modification of HsaD pre-incubated with $CyC_{7β}$ and $CyC_{31}$*** as determined by MALDI-TOF mass spectrometry. **(E) *Peptide mass fingerprint (1300-1900 Da zone) of the digested HsaD pre-incubated with $CyC_{7β}$ and $CyC_{31}$*** showing a signal corresponding to the modified catalytic peptide resulting from the covalent binding of each **CyC** to

the catalytic $Ser^{114}$ (*left panels*); and MS/MS spectrum of the modified $V^{108}PLVGNS^{114}LGGGTAVR^{122}$ peptide (*right panels*). The sequence of each peptide is shown from C-terminal to N-Terminal (from left to right) with a gap at the $Ser^{114}$ place corresponding to the remaining Serine structure without the hydroxyl moiety (~ 69 Da) and the neutral loss corresponding to **CyC$_{7\beta}$** and **CyC$_{31}$** binding, thus confirming the covalent adduct. **(F)** ***Mechanism of HsaD inhibition by the phosphonate CyC$_{7\beta}$ and the phosphate analog CyC$_{31}$*** based on mass spectrometry analyses. a.u., arbitrary units.

**Fig. 3**. **Peptide mass fingerprint (1300-1900 Da zone) of the digested HsaD pre-incubated with (A) CyC$_{8\beta}$ and (B) CyC$_{17}$** showing a signal corresponding to the modified catalytic peptide resulting from the covalent binding of each **CyC** to the catalytic $Ser^{114}$ (*left panels*); and MS/MS spectrum of the modified $V^{108}PLVGNS^{114}LGGGTAVR^{122}$ peptide (*right panels*). The sequence of each peptide is shown from C-terminal to N-Terminal (from left to right) with a gap at the $Ser^{114}$ place corresponding to the remaining Serine structure without the hydroxyl moiety (~ 69 Da) and the neutral loss corresponding to **CyC$_{8\beta}$** and **CyC$_{17}$** binding, thus confirming the covalent adduct.

**Fig. 4. Comparison of native HsaD and HsaD-CyC crystal structures. (A)** ***Superposition of the crystal structures of native HsaD and HsaD in complex with the different CyC compounds.*** Native HsaD is in light grey cartoon, HsaD in complex with **CyC$_{7\beta}$**, **CyC$_{8\beta}$**, **CyC$_{17}$** and **CyC$_{31}$** are in blue, purple, orange and pink, respectively. For clarity, the coordinates of the **CyC** compounds have been omitted **(B)** ***Close up view of the HsaD active site.*** The catalytic residues $Ser^{114}$, $Asp^{241}$ and $His^{269}$ are shown as sticks, the active site residues displaying conformational changes are shown as lines. **(C)** ***Close up view*** comparing the superposed structures of native HsaD, HsaD-**CyC$_{8\beta}$**, HsaD-**CyC$_{17}$**, and HsaD-**CyC$_{31}$** (*left*) as well as the structure of HsaD-**CyC$_{7\beta}$** (*right*), showing the fusion of two helices into one in the latter complex. Structures were drawn with PyMOL Molecular Graphics System (Version 2, Schrödinger, LLC).

**Fig. 5. Structural characterization of HsaD-CyC complexes. (A)** ***2Fo-Fc electron density maps for two HsaD-CyC complexes.*** Ligands are depicted with green sticks and the catalytic $Ser^{114}$ with blue and pink sticks for the HsaD-**CyC$_{7\beta}$** and HsaD-**CyC$_{31}$** complexes, respectively. Density maps are contoured at 1σ level. **(B)** ***Ligplot+ representation of the HsaD-CyC$_{7\beta}$ (left) and HsaD-CyC$_{31}$ (right) complexes.*** Hydrogen-bonds, hydrophobic interactions and the covalent $Ser^{114}$-**CyC** bond are shown. **(C)** ***X-ray structures of CyC compounds bound to HsaD.*** **CyC$_{7\beta}$** (*top*), **CyC$_{31}$** (*bottom*) and the catalytic $Ser^{114}$ are shown as sticks, the protein surface is colored in grey with hydrophobic residues highlighted in pale orange. **(D)** ***Close-up view of HsaD active site containing the bound***

***inhibitors.*** **CyC$_{7\beta}$** (*top*), **CyC$_{31}$** (*bottom*) and the main active site residues are shown as sticks. Red dashes represent hydrogen bonds, water molecules are represented by red spheres. Structures were drawn with PyMOL Molecular Graphics System (Version 2, Schrödinger, LLC).

**Fig. 6.** ***In silico*** **molecular docking experiments. (A)** ***Top-scoring docking position of CyC$_{32}$*** (green) with the crystal structure of HsaD in van der Waals surface representation. Hydrophobic residues are highlighted in bright orange. **(B)** ***Distances between the catalytic Ser$^{114}$-Oγ residue and the CyC reactive phosphorus atom.*** The distances were calculated from the top-scoring docking positions of **CyC$_{32}$** (green) and **CyC$_{31docked}$** (white). **(C-D)** ***Top-scoring docking position of CyC$_{31docked}$ and CyC$_{17}$.*** Superimposition of the top-scoring docking position of **CyC$_{31docked}$** (white - **C**) and **CyC$_{17}$** [16] (cyan – **D**) with the crystal structure of S$^{114}$-**CyC$_{31}$** (yellow). Each inhibitor is in stick representation with the following atom color-code: oxygen, red; phosphorus, orange; carbon, green, white, yellow or cyan. The catalytic Ser$^{114}$ residue is colored in magenta. Structures were drawn with PyMOL Molecular Graphics System (Version 1.4, Schrödinger, LLC) using the PDB file 7ZM4.

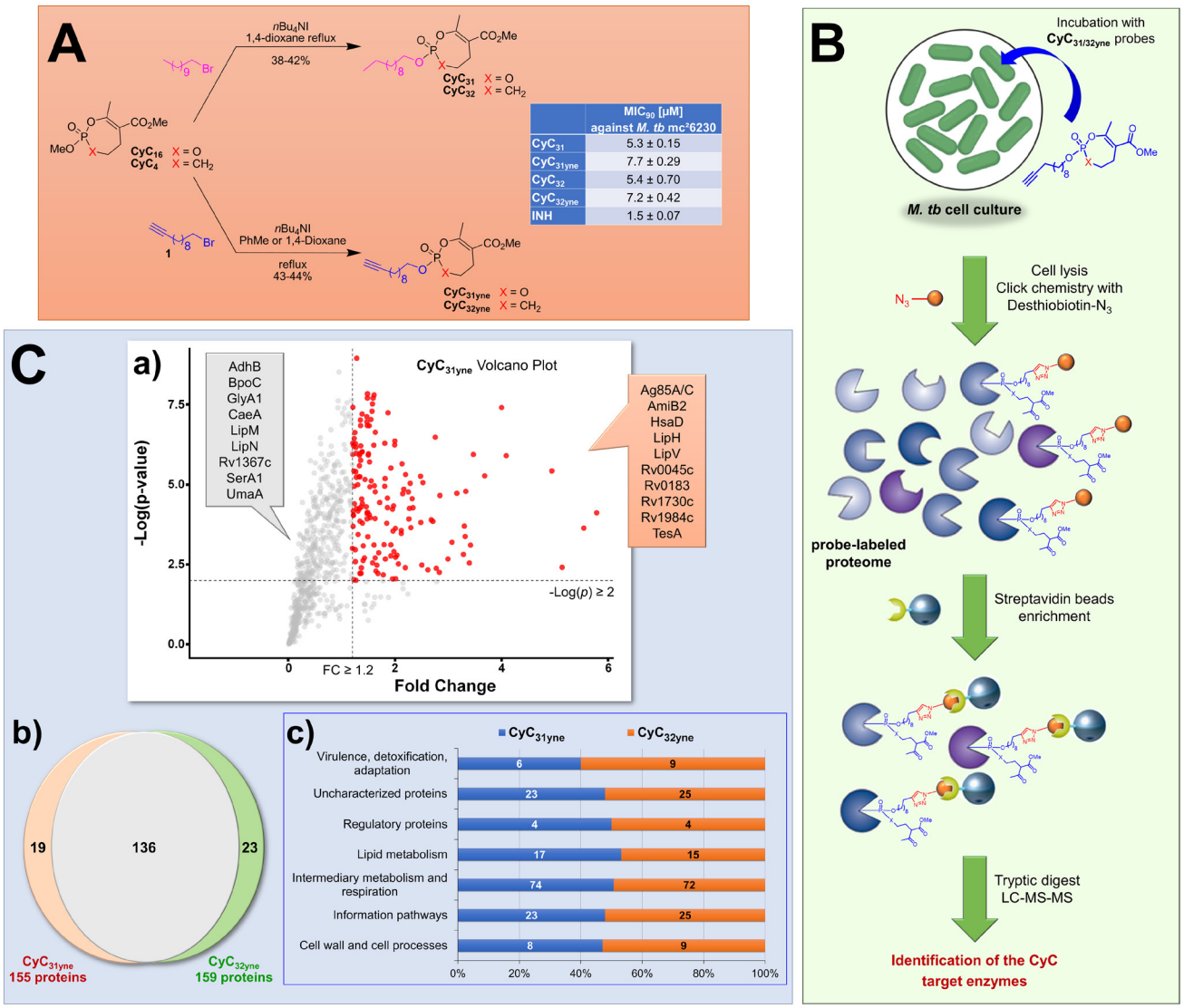
A
nBu4NI
1,4-dioxane reflux
38-42%
CycC31 X = O
CycC32 X = CH2
CycC16 X = O
CycC4 X = CH2
nBu4NI
PhMe or 1,4-Dioxane
reflux
43-44%
CycC31yne X = O
CycC32yne X = CH2
MIC90 [µM] against M. tb mc²6230
CycC31 5.3 ± 0.15
CycC31yne 7.7 ± 0.29
CycC32 5.4 ± 0.70
CycC32yne 7.2 ± 0.42
INH 1.5 ± 0.07
B
Incubation with CycC31/32yne probes
M. tb cell culture
Cell lysis
Click chemistry with Desthiobiotin-N3
probe-labeled proteome
Streptavidin beads enrichment
Tryptic digest LC-MS-MS
Identification of the CyC target enzymes
C
a)
CycC31yne Volcano Plot
AdhB
BpoC
GlyA1
CaeA
LipM
LipN
Rv1367c
SerA1
UmaA
Ag85A/C
AmiB2
HsaD
LipH
LipV
Rv0045c
Rv0183
Rv1730c
Rv1984c
TesA
-Log(p-value)
-Log(p) ≥ 2
FC ≥ 1.2
Fold Change
b)
19
136
23
CycC31yne 155 proteins
CycC32yne 159 proteins
c)
CycC31yne
CycC32yne
Virulence, detoxification, adaptation 6 9
Uncharacterized proteins 23 25
Regulatory proteins 4 4
Lipid metabolism 17 15
Intermediary metabolism and respiration 74 72
Information pathways 23 25
Cell wall and cell processes 8 9
0% 20% 40% 60% 80% 100%

**Figure 1**

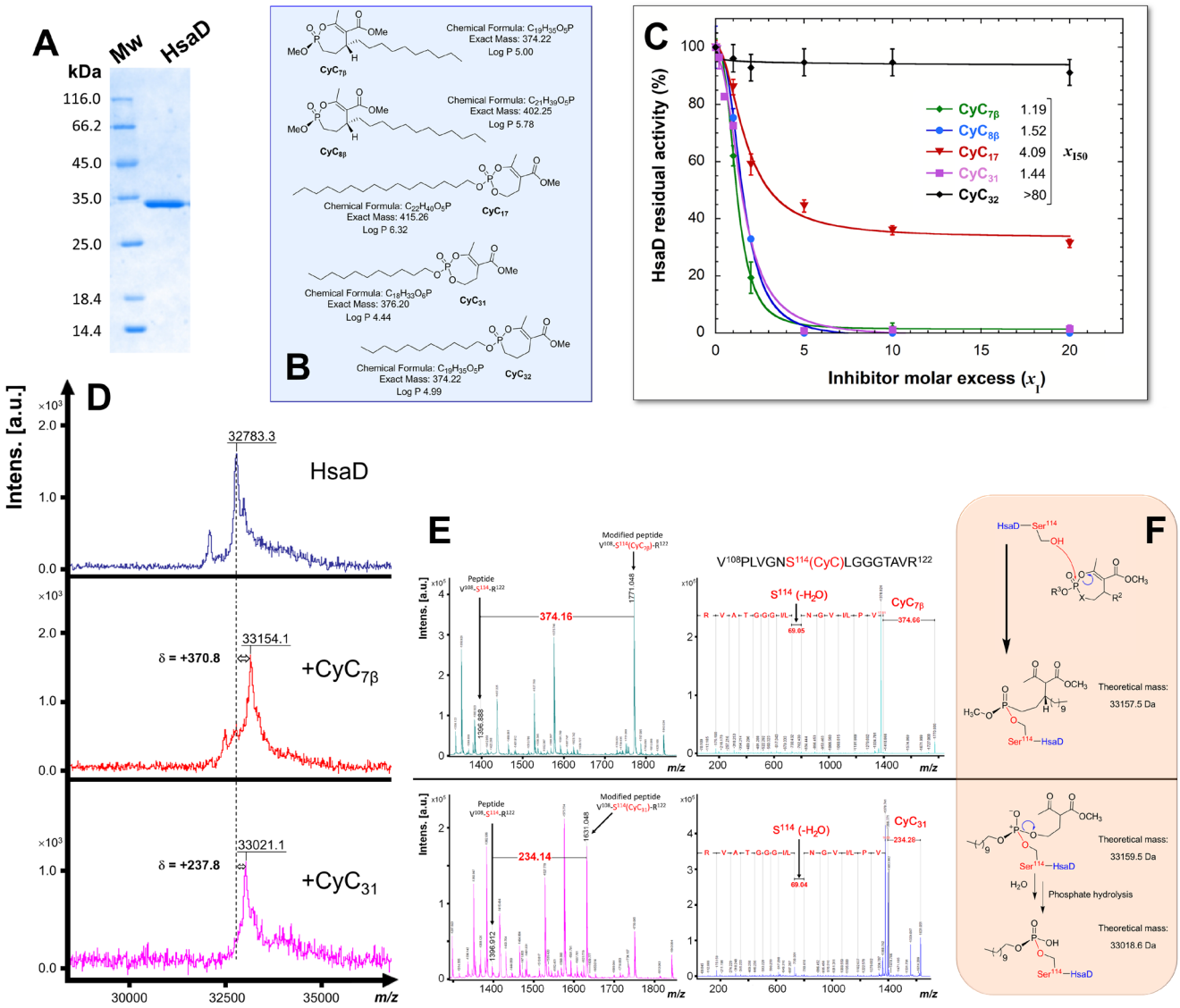
A
Mw
HsaD
kDa
116.0
66.2
45.0
35.0
25.0
18.4
14.4
B
Chemical Formula: C19H35O5P
Exact Mass: 374.22
Log P 5.00
CyC7β
Chemical Formula: C21H39O5P
Exact Mass: 402.25
Log P 5.78
CyC8β
Chemical Formula: C22H40O5P
Exact Mass: 415.26
Log P 6.32
CyC17
Chemical Formula: C18H33O5P
Exact Mass: 376.20
Log P 4.44
CyC31
Chemical Formula: C19H35O5P
Exact Mass: 374.22
Log P 4.99
CyC32
C
HsaD residual activity (%)
Inhibitor molar excess (xI)
CyC7β 1.19
CyC8β 1.52
CyC17 4.09
CyC31 1.44
CyC32 >80
x150
D
Intens. [a.u.]
32783.3
HsaD
δ = +370.8
33154.1
+CyC7β
δ = +237.8
33021.1
+CyC31
m/z
E
Peptide V108-S114-R122
Modified peptide V108-S114(CyC7β)-R122
374.16
1396.888
1771.048
V108PLVGNS114(CyC)LGGGTAVR122
S114 (-H2O)
69.05
CyC7β
374.66
Modified peptide V108-S114(CyC31)-R122
234.14
1396.912
1631.048
CyC31
234.28
69.04
F
HsaD—Ser114
Theoretical mass:
33157.5 Da
Ser114—HsaD
Theoretical mass:
33159.5 Da
H2O
Phosphate hydrolysis
Theoretical mass:
33018.6 Da

**Figure 2**

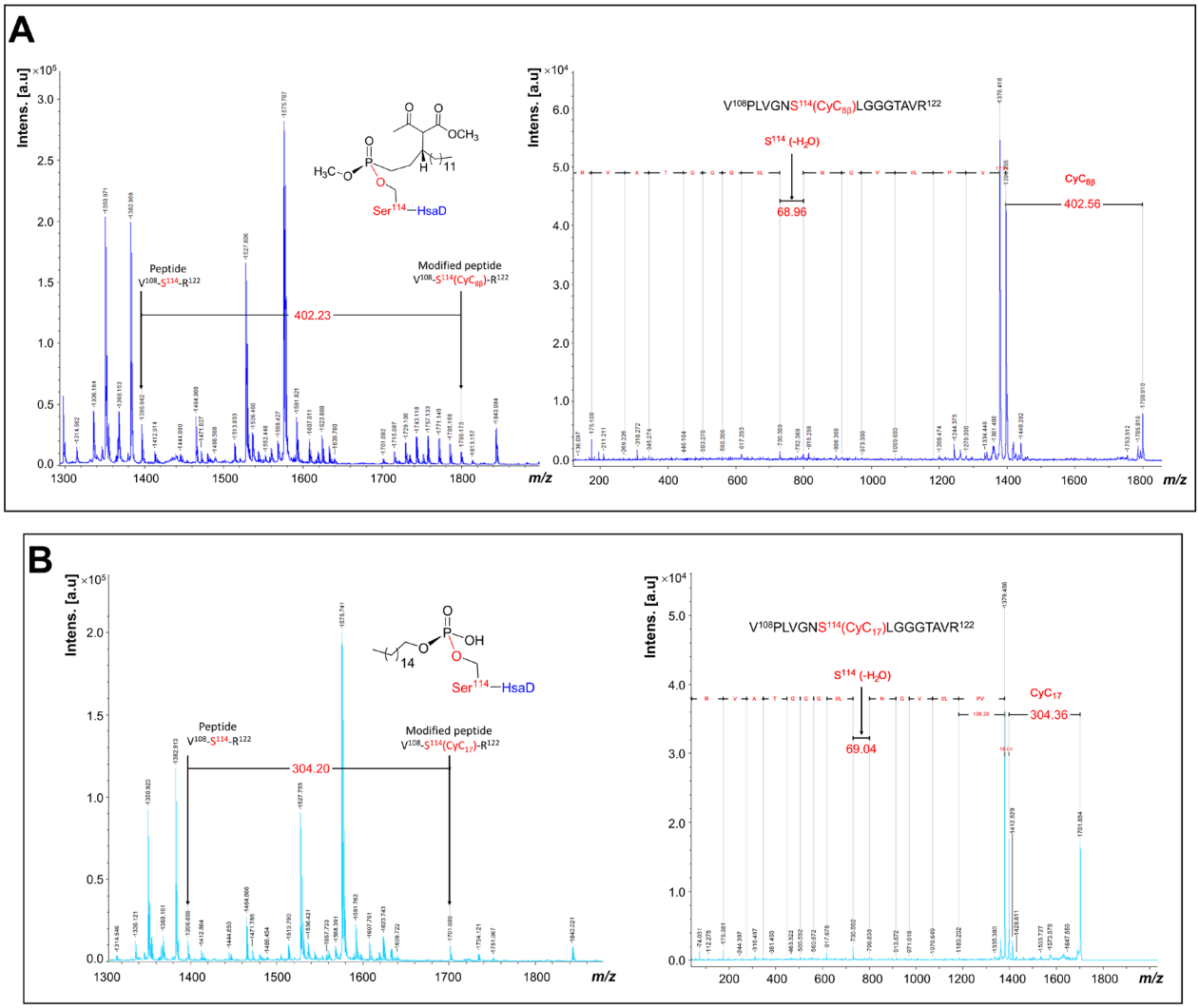
A
Intens. [a.u]
Peptide
V108-S114-R122
Modified peptide
V108-S114(CyC8β)-R122
402.23
Ser114—HsaD
V108PLVGNS114(CyC8β)LGGGTAVR122
S114 (-H2O)
68.96
CyC8β
402.56
m/z
B
Intens. [a.u]
Peptide
V108-S114-R122
Modified peptide
V108-S114(CyC17)-R122
304.20
Ser114—HsaD
V108PLVGNS114(CyC17)LGGGTAVR122
S114 (-H2O)
69.04
CyC17
304.36
m/z

**Figure 3**

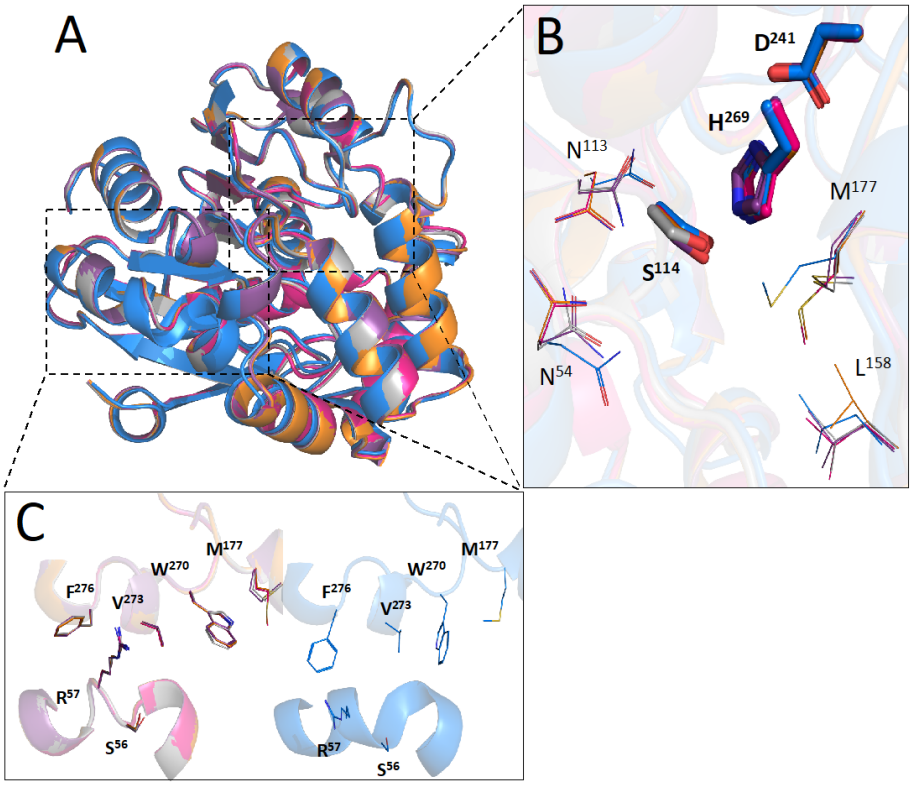
A
B
D241
H269
N113
M177
S114
N54
L158
C
M177
W270
F276
V273
R57
S56
M177
W270
F276
V273
R57
S56

**Figure 4**

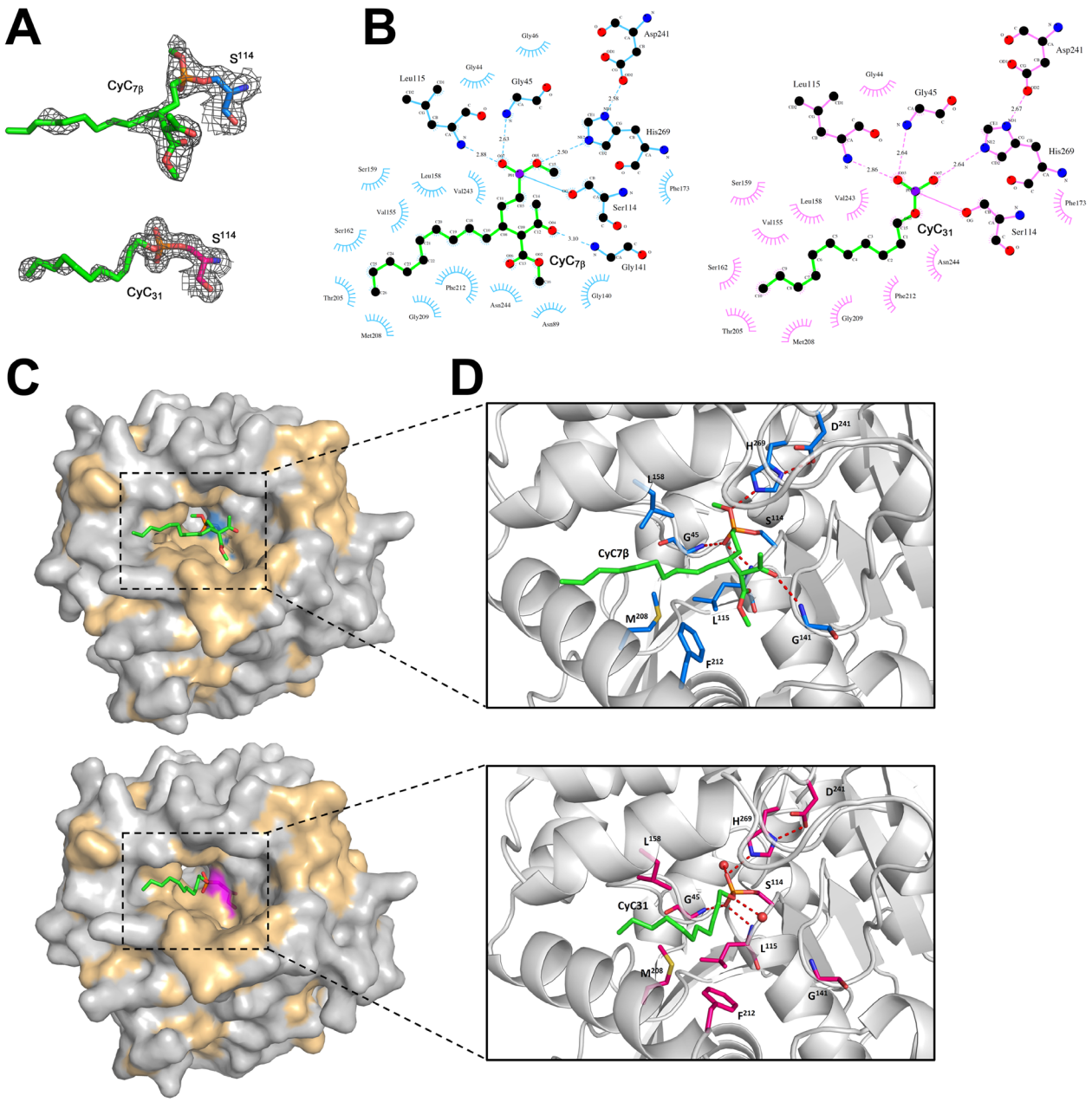
A
S114
CyC7β
S114
CyC31
B
Asp241
Gly46
Gly44
Leu115
Gly45
His269
Ser159
Leu158
Val243
Phe173
Val155
Ser114
Ser162
CyC7β
Gly141
Thr205
Phe212
Asn244
Gly209
Gly140
Asn89
Met208
Asp241
Gly44
Leu115
Gly45
His269
Ser159
Leu158
Val243
Val155
CyC31
Ser114
Phe173
Asn244
Ser162
Phe212
Thr205
Gly209
Met208
C
D
D241
H269
L158
S114
G45
CyC7β
M208
L115
G141
F212
D241
H269
L158
S114
G45
CyC31
L115
M208
G141
F212

**Figure 5**

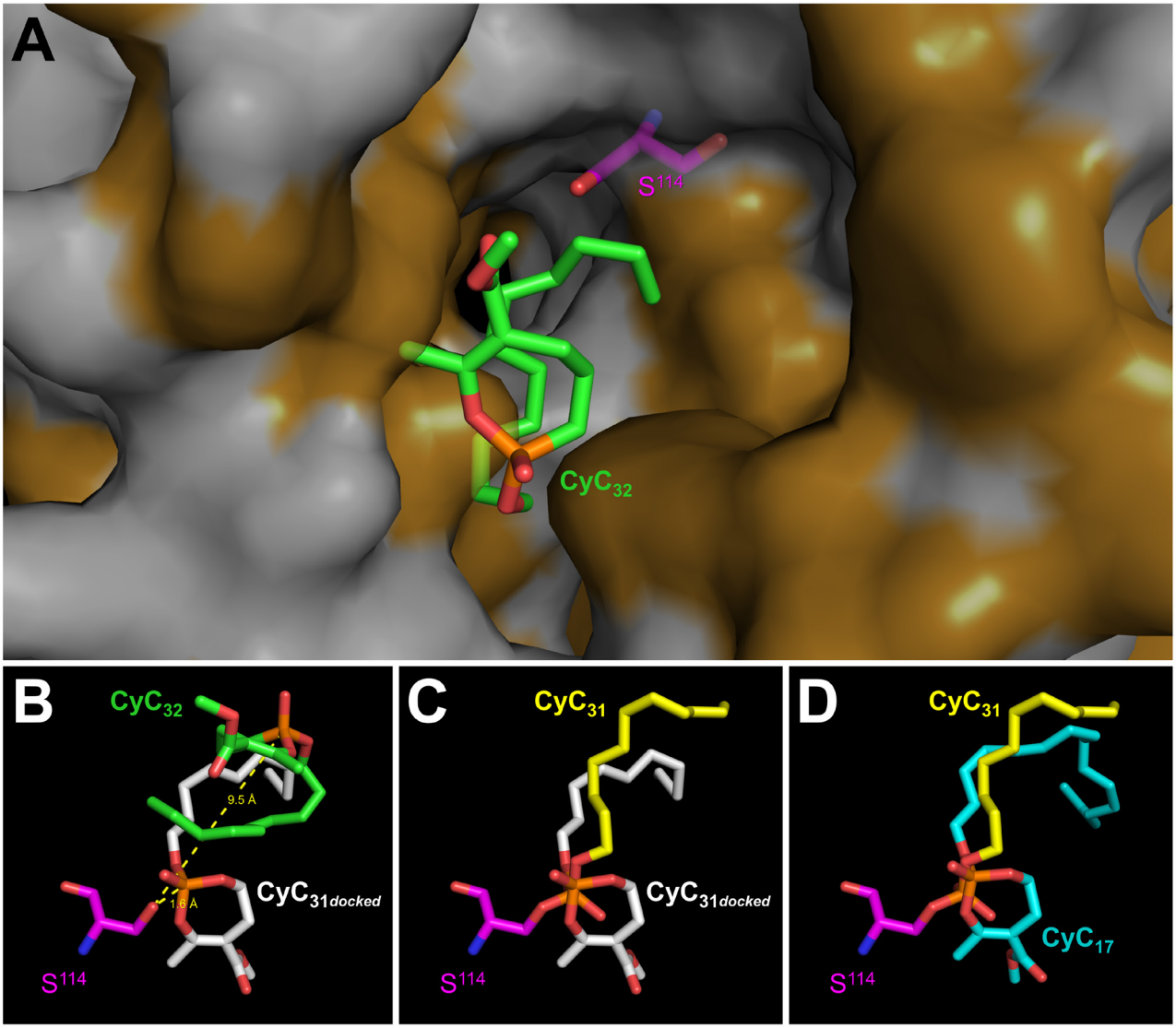
A
S114
CyC32
B
CyC32
9.5 Å
1.6 Å
CyC31docked
S114
C
CyC31
CyC31docked
S114
D
CyC31
CyC17
S114

**Figure 6**